LEARNING ENERGY-BASED MODELS BY COOPERATIVE DIFFUSION RECOVERY LIKELIHOOD

Yaxuan Zhu
UCLA
yaxuanzhu@g.ucla.edu

Jianwen Xie
Akool Research
jianwen@ucla.edu

Ying Nian Wu
UCLA
ywu@stat.ucla.edu

Ruiqi Gao
Google DeepMind
ruiqig@google.com

ABSTRACT

Training energy-based models (EBMs) on high-dimensional data can be both challenging and time-consuming, and there exists a noticeable gap in sample quality between EBMs and other generative frameworks like GANs and diffusion models. To close this gap, inspired by the recent efforts of learning EBMs by maximizing diffusion recovery likelihood (DRL), we propose cooperative diffusion recovery likelihood (CDRL), an effective approach to tractably learn and sample from a series of EBMs defined on increasingly noisy versions of a dataset, paired with an initializer model for each EBM. At each noise level, the two models are jointly estimated within a cooperative training framework: samples from the initializer serve as starting points that are refined by a few MCMC sampling steps from the EBM. The EBM is then optimized by maximizing recovery likelihood, while the initializer model is optimized by learning from the difference between the refined samples and the initial samples. In addition, we made several practical designs for EBM training to further improve the sample quality. Combining these advances, our approach significantly boost the generation performance compared to existing EBM methods on CIFAR-10 and ImageNet datasets. We also demonstrate the effectiveness of our models for several downstream tasks, including classifier-free guided generation, compositional generation, image inpainting and out-of-distribution detection.

1 INTRODUCTION

Energy-based models (EBMs), as a class of probabilistic generative models, have exhibited their flexibility and practicality in a variety of application scenarios, such as realistic image synthesis (Xie et al., 2016; 2018a; Nijkamp et al., 2019; Du & Mordatch, 2019; Arbel et al., 2021; Hill et al., 2022; Xiao et al., 2021; Lee et al., 2023; Grathwohl et al., 2021; Cui & Han, 2023), graph generation (Liu et al., 2021), compositional generation (Du et al., 2020; 2023), video generation (Xie et al., 2021c), 3D generation (Xie et al., 2021a; 2018b), simulation-based inference (Glaser et al., 2022), stochastic optimization (Kong et al., 2022), out-of-distribution detection (Grathwohl et al., 2020; Liu et al., 2020), and latent space modeling (Pang et al., 2020; Zhu et al., 2023; Zhang et al., 2023; Yu et al., 2023). Despite these successes of EBMs, training and sampling from EBMs remains challenging, mainly due of the intractability of the partition function in the distribution.

Recently, Diffusion Recovery Likelihood (DRL) (Gao et al., 2021) has emerged as a powerful framework for estimating EBMs. Inspired by diffusion models (Sohl-Dickstein et al., 2015; Ho et al., 2020; Song & Ermon, 2019), DRL assumes a sequence of EBMs for the marginal distributions of samples perturbed by a Gaussian diffusion process, where each EBM is trained with recovery likelihood that maximizes the conditional probability of the data at the current noise level given their noisy versions at a higher noise level. Compared to the regular likelihood, Maximizing recovery likelihood is more tractable, as sampling from the conditional distribution is much easier than sampling from the marginal distribution. DRL achieves exceptional generation performance among EBM-based generative models. However, a noticeable performance gap still exists between the sample quality of EBMs and other generative frameworks like GANs or diffusion models. Moreover, DRL requires around 30 MCMC sampling steps at each noise level to generate valid samples, which can be time-consuming during both training and sampling processes.

To further close the performance gap and expedite EBM training and sampling with fewer MCMC sampling steps, we introduce Cooperative Diffusion Recovery Likelihood (CDRL), that jointly estimates a sequence of EBMs and MCMC initializers defined on data perturbed by a diffusion process. At each noise level, the initializer and EBM are updated by a cooperative training scheme (Xie et al., 2018a): The initializer model proposes initial samples by predicting the samples at the current noise level given their noisy versions at a higher noise level. The initial samples are then refined by a few MCMC sampling steps from the conditional distribution defined by the EBM. Given the refined samples, the EBM is updated by maximizing recovery likelihood, and the initializer is updated to absorb the difference between the initial samples and the refined samples. The introduced initializer models learn to accumulate the MCMC transitions of the EBMs, and reproduce them by direct ancestral sampling. Combining with a new noise schedule and a variance reduction technique, we achieve significantly better performance than the existing methods of estimating EBMs. We further incorporate classifier-free guidance (CFG) (Ho & Salimans, 2022) to enhance the performance of conditional generation, and we observe similar trade-offs between sample quality and sample diversity as CFG for diffusion models when adjusting the guidance strength. In addition, we showcase that our approach can be applied to perform several useful downstream tasks, including compositional generation, image inpainting and out-of-distribution detection.

Our main contributions are as follows: (1) We propose cooperative diffusion recovery likelihood (CDRL) that tractably and efficiently learns and samples from a sequence of EBMs and MCMC initializers; (2) We make several practical design choices related to noise scheduling, MCMC sampling, noise variance reduction for EBM training; (3) Empirically we demonstrate that CDRL achieves significant improvements on sample quality compared to existing EBM approaches, on CIFAR-10 and ImageNet 32×32 datasets; (4) We show that CDRL has great potential to enable more efficient sampling with sampling adjustment techniques; (5) We demonstrate CDRL's ability in compositional generation, image inpainting and out-of-distribution (OOD) detection, as well as its compatibility with classifier-free guidance for conditional generation.

2 Preliminaries on Energy-Based Models

Let $\mathbf{x} \sim p_{\text{data}}(\mathbf{x})$ be a training example from an underlying data distribution. An energy-based model defines the density of $\mathbf{x}$ by

$$p_\theta(\mathbf{x}) = \frac{1}{Z_\theta} \exp(f_\theta(\mathbf{x})), \tag{1}$$

where f_θ is the unnormalized log density, or negative energy, parametrized by a neural network with a scalar output. Z_θ is the normalizing constant or partition function. The derivative of the log-likelihood function of an EBM can be approximately written as

$$\mathcal{L}'(\theta) = \mathbb{E}_{p_{\text{data}}} \left[\frac{\partial}{\partial \theta} f_\theta(\mathbf{x}) \right] - \mathbb{E}_{p_\theta} \left[\frac{\partial}{\partial \theta} f_\theta(\mathbf{x}) \right], \tag{2}$$

where the second term is analytically intractable and has to be estimated by Monte Carlo samples from the current model p_θ. Therefore, applying gradient-based optimization for an EBM usually involves an inner loop of MCMC sampling, which can be time-consuming for high-dimensional data.

3 Cooperative Diffusion Recovery Likelihood

3.1 Diffusion recovery likelihood

Given the difficulty of sampling from the marginal distribution $p(\mathbf{x})$ defined by an EBM, we could instead estimate a sequence of EBMs defined on increasingly noisy versions of the data and jointly estimate them by maximizing *recovery likelihood*. Specifically, assume a sequence of noisy training examples perturbed by a Gaussian diffusion process: $\mathbf{x}_0, \mathbf{x}_1, ..., \mathbf{x}_T$ such that $\mathbf{x}_0 \sim p_{\text{data}}$; $\mathbf{x}_{t+1} = \alpha_{t+1}\mathbf{x}_t + \sigma_{t+1}\boldsymbol{\epsilon}$. Denote $\mathbf{y}_t = \alpha_{t+1}\mathbf{x}_t$ for notation simplicity. The marginal distributions of $\{\mathbf{y}_t; t = 1, ..., T\}$ are modeled by a sequence of EBMs: $p_\theta(\mathbf{y}_t) = \frac{1}{Z_{\theta,t}} \exp(f_\theta(\mathbf{y}_t; t))$. Then the conditional EBM of $\mathbf{y}_t$ given the sample $\mathbf{x}_{t+1}$ at a higher noise level can be derived as

$$p_\theta(\mathbf{y}_t|\mathbf{x}_{t+1}) = \frac{1}{\tilde{Z}_{\theta,t}(\mathbf{x}_{t+1})} \exp\left(f_\theta(\mathbf{y}_t; t) - \frac{1}{2\sigma_{t+1}^2} \|\mathbf{y}_t - \mathbf{x}_{t+1}\|^2 \right), \tag{3}$$

where $\tilde{Z}_{\theta,t}(\mathbf{x}_{t+1})$ is the partition function of the conditional EBM dependent on $\mathbf{x}_{t+1}$. Compared with the marginal EBM $p_\theta(\mathbf{y}_t)$, when σ_{t+1} is small, the extra quadratic term in $p_\theta(\mathbf{y}_t|\mathbf{x}_{t+1})$ constrains the conditional energy landscape to be localized around $\mathbf{x}_{t+1}$, making the latter less multi-modal and easier to sample from with MCMC. In the extreme case when σ_{t+1} is infinitesimal, $p_\theta(\mathbf{y}_t|\mathbf{x}_{t+1})$ is approximately a Gaussian distribution that can be tractably sampled from and has a close connection to diffusion models (Gao et al., 2021). In the other extreme case when $\sigma_{t+1} \to \infty$, the conditional distribution falls back to the marginal distribution, and we lose the advantage of being more MCMC friendly for the conditional distribution. Therefore, we need to maintain a small σ_{t+1} between adjacent time steps, and to equip the model with the ability of generating new samples from white noises, we end up with estimating a sequence of EBMs defined on the diffusion process. We use the variance-preserving noise schedule (Song et al., 2021b), under which case we have $\mathbf{x}_t = \bar{\alpha}_t \mathbf{x}_0 + \bar{\sigma}_t \boldsymbol{\epsilon}$, where $\bar{\alpha}_t = \prod_{t=1}^{T} \alpha_t$ and $\bar{\sigma}_t = \sqrt{1 - \bar{\alpha}_t^2}$.

We estimate each EBM by maximizing the following recovery log-likelihood function at each noise level (Bengio et al., 2013):

$$\mathcal{J}_t(\theta) = \frac{1}{n} \sum_{i=1}^{n} \log p_\theta(\mathbf{y}_{t,i}|\mathbf{x}_{t+1,i}), \tag{4}$$

where $\{\mathbf{y}_{t,i}, \mathbf{x}_{t+1,i}\}$ are pair of samples at time steps t and $t+1$. Sampling from $p_\theta(\mathbf{y}_t|\mathbf{x}_{t+1})$ can be achieved by running K steps of Langevin dynamics from the initialization point $\tilde{\mathbf{y}}_t^0 = \mathbf{x}_{t+1,i}$ and iterating

$$\tilde{\mathbf{y}}_t^{\tau+1} = \tilde{\mathbf{y}}_t^{\tau} + \frac{s_t^2}{2} \left(\nabla_{\mathbf{y}} f_\theta(\tilde{\mathbf{y}}_t^{\tau}; t) - \frac{1}{\sigma_{t+1}^2} (\tilde{\mathbf{y}}_t^{\tau} - \mathbf{x}_{t+1}) \right) + s_t \boldsymbol{\epsilon}^{\tau}, \tag{5}$$

where s_t is the step size and τ is the index of MCMC sampling step. With the samples, the updating of EBMs then follows the same learning gradients as MLE (Equation 2), as the extra quadratic term $-\frac{1}{2\sigma_{t+1}^2}\|\mathbf{y}_t - \mathbf{x}_{t+1}\|^2$ in $p_\theta(\mathbf{y}_t|\mathbf{x}_{t+1})$ does not involve learnable parameters. It is worth noting that maximizing recovery likelihood still guarantees an unbiased estimator of the true parameters of the *marginal distribution* of the data.

3.2 Amortizing MCMC sampling with initializer models

Although $p_\theta(\mathbf{y}_t|\mathbf{x}_{t+1})$ is easier to sample from than $p_\theta(\mathbf{y}_t)$, when σ_{t+1} is not infinitesimal, the initialization of MCMC sampling, $\mathbf{x}_{t+1}$, may still be far from the data manifold of $\mathbf{y}_t$. This necessitates a certain amount of MCMC sampling steps at each noise level (e.g., 30 steps of Langevin dynamics in Gao et al. (2021)). Naively reducing the number of sampling steps would lead to training divergence or performance degradation.

To address this issue, we propose to learn an initializer model jointly with the EBM at each noise level, which maps $\mathbf{x}_{t+1}$ closer to the manifold of $\mathbf{y}_t$. Our work is inspired by the CoopNets (Xie et al., 2018a; 2021b; 2022b), which shows that jointly training a top-down generator via MCMC teaching will help the training of a single EBM model. We take this idea and generalize it to the recovery-likelihood model. More discussions are included in Appendix A. Specifically, the initializer model at noise level t is defined as

$$q_\phi(\mathbf{y}_t|\mathbf{x}_{t+1}) \sim \mathcal{N}(\boldsymbol{g}_\phi(\mathbf{x}_{t+1}; t), \tilde{\sigma}_t^2 \boldsymbol{I}). \tag{6}$$

It serves as a coarse approximation to $p_\theta(\mathbf{y}_t|\mathbf{x}_{t+1})$, as the former is a single-mode Gaussian distribution while the latter can be multi-modal. A more general formulation would be to involve latent variables $\mathbf{z}_t$ following a certain simple prior $p(\mathbf{z}_t)$ into $\boldsymbol{g}_\phi$. Then $q_\phi(\mathbf{y}_t, t|\mathbf{x}_{t+1}) = \mathbb{E}_{p(\mathbf{z}_t)}\left[q_\phi(\mathbf{y}_t, \mathbf{z}_t, t|\mathbf{x}_{t+1})\right]$ can be non-Gaussian (Xiao et al., 2022). However, we empirically find that the simple initializer in Equation 6 works well. Compared with the more general formulation, the simple initializer avoids the inference of $\mathbf{z}_t$ which may again require MCMC sampling, and leads to more stable training. Different from Xiao et al. (2022), samples from the initializer just serves as the starting points and are refined by sampling from the EBM, instead of being treated as the final samples. We follow (Ho et al., 2020) to set $\tilde{\sigma}_t = \sqrt{\frac{1-\bar{\alpha}_t^2}{1-\bar{\alpha}_{t+1}^2}}\sigma_t$. If we treat the sequence of initializers as the reverse process, such choice of $\tilde{\sigma}_t$ corresponds to the lower bound of the standard deviation given by p_{data} being a delta function (Sohl-Dickstein et al., 2015).

3.3 Cooperative training

We jointly train the sequence of EBMs and intializers in a cooperative fashion. Specifically, at each iteration, for a randomly sampled noise level t, we obtain an initial sample $\hat{\mathbf{y}}_t$ from the intializer model. Then a synthesized sample $\tilde{\mathbf{y}}_t$ from $p(\mathbf{y}_t|\mathbf{x}_{t+1})$ is generated by initializing from $\hat{\mathbf{y}}_t$ and running a few steps of Langevin dynamics (Equation 5). The parameters of EBM are then updated by maximizing the recovery log-likelihood function (Equation 4). The learning gradient of EBM is

$$\nabla_\theta \mathcal{J}_t(\theta) = \nabla_\theta \left[\frac{1}{n} \sum_{i=1}^{n} f_\theta(\mathbf{y}_{t,i}; t) - \frac{1}{n} \sum_{i=1}^{n} f_\theta(\tilde{\mathbf{y}}_{t,i}; t) \right]. \tag{7}$$

To train the intializer model that amortizes the MCMC sampling process, we treat the revised sample $\tilde{\mathbf{y}}_t$ by the EBM as the observed data of the initializer model, and estimate the parameters of the initializer by maximizing log-likelihood:

$$\mathcal{L}_t(\phi) = \frac{1}{n} \sum_{i=1}^{n} \left[-\frac{1}{2\tilde{\sigma}_t^2} \|\tilde{\mathbf{y}}_{t,i} - \boldsymbol{g}_\phi(\mathbf{x}_{t+1,i}; t)\|^2 \right]. \tag{8}$$

That is, the initializer model learns to absorb the difference between $\hat{\mathbf{y}}_t$ and $\tilde{\mathbf{y}}_t$ at each iteration so that $\hat{\mathbf{y}}_t$ is getting closer to the samples from $p_\theta(\mathbf{y}_t|\mathbf{x}_{t+1})$. In practice, we re-weight $\mathcal{L}_t(\phi)$ across different noise levels by removing the coefficient $\frac{1}{2\tilde{\sigma}_t^2}$, similar to the “simple loss" in diffusion models. The training algorithm is summarized in Algorithm 1.

After training, we generate new samples by starting from Gaussian white noise and progressively samples $p_\theta(\mathbf{y}_t|\mathbf{x}_{t+1})$ at decreasingly lower noise levels. For each noise level, an initial proposal is generated from the intializer model, followed by a few steps of Langevin dynamics from the EBM. See Algorithm 2 for a summary.

3.4 Noise variance reduction

We further propose a simple way to reduce the variance of training gradients. In principle, the pair of $\mathbf{x}_t$ (or $\mathbf{y}_t$) and $\mathbf{x}_{t+1}$ is generated by $\mathbf{x}_t \sim \mathcal{N}(\bar{\alpha}_t \mathbf{x}_0, \bar{\sigma}_t^2 \boldsymbol{I})$ and $\mathbf{x}_{t+1} \sim \mathcal{N}(\alpha_{t+1} \mathbf{x}_t, \sigma_{t+1}^2 \boldsymbol{I})$. Alternatively, we can fix the Gaussian white noise $\mathbf{e} \sim \mathcal{N}(0, \boldsymbol{I})$, and sample pair $(\mathbf{x}'_t, \mathbf{x}'_{t+1})$ by

$$\begin{aligned} \mathbf{x}'_t &= \bar{\alpha}_t \mathbf{x}_0 + \bar{\sigma}_t \mathbf{e} \\ \mathbf{x}'_{t+1} &= \bar{\alpha}_{t+1} \mathbf{x}'_t + \bar{\sigma}_{t+1} \mathbf{e}. \end{aligned} \tag{9}$$

In other words, both $\mathbf{x}'_t$ and $\mathbf{x}'_{t+1}$ are linear interpolation between the clean sample $\mathbf{x}_0$ and a sampled white noise image $\mathbf{e}$. $\mathbf{x}'_t$ and $\mathbf{x}'_{t+1}$ have the same marginal distributions as $\mathbf{x}_t$ and $\mathbf{x}_{t+1}$. But $\mathbf{x}'_t$ is deterministic given $\mathbf{x}_0$ and $\mathbf{x}'_{t+1}$, while there’s still variance for $\mathbf{x}_t$ given $\mathbf{x}_0$ and $\mathbf{x}_{t+1}$. This schedule is related to the ODE forward process used in flow matching (Lipman et al., 2022) and rectified flow (Liu et al., 2022b).

3.5 Conditional generation and classifier-free guidance

Ho & Salimans (2022) introduced classifier-free guidance, which greatly enhances the sample quality of conditional diffusion models and balances between sample quality and diversity by adjusting the strength of guidance. Given the close connection between EBMs and diffusion models, we show that it is possible to apply classifier-free guidance in our CDRL as well. Specifically, suppose c is the context (e.g., a label or a text description). At each noise level we jointly estimate an unconditional EBM $p_\theta(\mathbf{y}_t) \propto \exp(f_\theta(\mathbf{y}_t; t))$ and a conditional EBM $p_\theta(\mathbf{y}_t|c) \propto \exp(f_\theta(\mathbf{y}_t; c, t))$. By following the classifier-free guidance (Ho & Salimans, 2022), we can perform conditional sampling using the following linear combination of the conditional and unconditional gradients:

$$\begin{aligned} \nabla_{\mathbf{y}} \log \tilde{p}_\theta(\mathbf{y}_t|c) &= (w+1) \nabla_{\mathbf{y}} \log p_\theta(\mathbf{y}_t; c, t) - w \nabla_{\mathbf{y}} \log p_\theta(\mathbf{y}_t; t) && (10) \\ &= (w+1) \nabla_{\mathbf{y}} f_\theta(\mathbf{y}_t; c, t) - w \nabla_{\mathbf{y}} f_\theta(\mathbf{y}_t; t), && (11) \end{aligned}$$

where w controls the guidance strength. We adopt a single neural network to parameterize both conditional and unconditional models, where for the unconditional model we can simply input a null token

```
**Algorithm 1** CDRL Training
**Input**: (1) observed data $\mathbf{x}_0 \sim p_{\text{data}}(\mathbf{x})$; (2) Number of noise levels $T$; (3) Number of Langevin sampling steps $K$ per noise level; (4) Langevin step size at each noise level $s_t$; (5) Learning rate $\eta_\theta$ for EBM $f_\theta$; (6) Learning rate $\eta_\phi$ for initializer $g_\phi$;
**Output**: Parameters $\theta, \phi$
  Randomly initialize $\theta$ and $\phi$.
  repeat
      Sample noise level $t$ from $\{0, 1, ..., T-1\}$.
      Sample $\boldsymbol{\epsilon} \sim \mathcal{N}(0, \boldsymbol{I})$. Let $\mathbf{x}_{t+1} = \bar{\alpha}_{t+1}\mathbf{x}_0 + \bar{\sigma}_{t+1}\boldsymbol{\epsilon}$, $\mathbf{y}_t = \alpha_{t+1}(\bar{\alpha}_t\mathbf{x}_0 + \bar{\sigma}_t\boldsymbol{\epsilon})$.
      Generate the initial sample $\hat{\mathbf{y}}_t$ following Equation 6.
      Generate the refined sample $\mathbf{y}_t$ by running $K$ steps of Langevin dynamics starting from $\hat{\mathbf{y}}_t$ following Equation 5.
      Update EBM parameter $\theta$ following the gradients in Equation 7.
      Update initializer parameter $\phi$ by maximizing Equation 8.
  until converged
```

```
**Algorithm 2** CDRL Sampling
**Input**: (1) Number of noise levels $T$; (2) Number of Langevin sampling steps $K$ at each noise level; (3) Langevin step size at each noise level $\delta_t$; (4) Trained EBM $f_\theta$; (5) Trained initializer $g_\phi$;
**Output**: Samples $\tilde{\mathbf{x}}_0$
  Randomly initialize $\mathbf{x}_T \sim \mathcal{N}(0, \boldsymbol{I})$.
  for $t = T-1$ to $0$ do
      Generate initial proposal $\hat{\mathbf{y}}_t$ following Equation 6.
      Update $\hat{\mathbf{y}}_t$ to $\tilde{\mathbf{y}}_t$ by $K$ iterations of Equation 5.
      Let $\tilde{\mathbf{x}}_t = \tilde{\mathbf{y}}_t/\alpha_{t+1}$.
  end for
```

$\varnothing$ for the class condition c when outputing the negative energy, i.e. $f_\theta(\mathbf{y}_t; t) = f_\theta(\mathbf{y}_t; c = \varnothing, t)$. Similarly, for the initializer model, we jointly estimate an unconditional model $q_\phi(\mathbf{y}_t|\mathbf{x}_{t+1}) \sim \mathcal{N}(\boldsymbol{g}_\phi(\mathbf{x}_{t+1}; t), \tilde{\sigma}_t^2\boldsymbol{I})$ and a conditional model $q_\phi(\mathbf{y}_t|c, \mathbf{x}_{t+1}) \sim \mathcal{N}(\boldsymbol{g}_\phi(\mathbf{x}_{t+1}; c, t), \tilde{\sigma}_t^2\boldsymbol{I})$. We parameterize both models in a single neural network. Since both models follow Gaussian distributions, the scaled conditional distribution with classifier-free guidance is still a Gaussian distribution (Dhariwal & Nichol, 2021):

$$\tilde{q}_\phi(\mathbf{y}_t|c, \mathbf{x}_{t+1}) = \mathcal{N}\left((w+1)\boldsymbol{g}_\phi(\mathbf{x}_{t+1}; c, t) - w\boldsymbol{g}_\phi(\mathbf{x}_{t+1}; t), \tilde{\sigma}_t^2\boldsymbol{I}\right). \tag{12}$$

3.6 COMPOSITIONALITY IN ENERGY-BASED MODEL

One attractive property of EBMs is compositionality: one can combine multiple EBMs conditioned on individual concepts, and re-normalize it to create a new distribution conditioned on the intersection of those concepts. Specifically, considering two EBMs $p_\theta(\mathbf{x}|c_1) \propto \exp(f_\theta(\mathbf{x}; c_1))$ and $p_\theta(\mathbf{x}|c_2) \propto \exp(f_\theta(\mathbf{x}; c_2))$ that are conditioned on two separate concepts c_1 and c_2 respectively, Du et al. (2020); Lee et al. (2023) construct a new EBM conditioned on both concepts as $p_\theta(\mathbf{x}|c_1, c_2) \propto \exp(f_\theta(\mathbf{x}; c_1) + f_\theta(\mathbf{x}; c_2))$ based on the production of expert (Hinton, 2002). Specifically, suppose the two concepts c_1 and c_2 are conditionally independent given the observed example $\mathbf{x}$. Then we have

$$\begin{aligned}\log p_\theta(\mathbf{x}|c_1, c_2) &= \log p_\theta(c_1, c_2|\mathbf{x}) + \log p_\theta(\mathbf{x}) + \text{const.}\\ &= \log p_\theta(c_1|\mathbf{x}) + \log p_\theta(c_2|\mathbf{x}) + \log p_\theta(\mathbf{x}) + \text{const.}\\ &= \log p_\theta(\mathbf{x}|c_1) + \log p_\theta(\mathbf{x}|c_2) - \log p_\theta(\mathbf{x}) + \text{const.},\end{aligned}$$

where const. is a constant term independent of $\mathbf{x}$. The composition can be generalized to include an arbitrary number of concepts. Suppose we have M conditionally independent concepts, then

$$\log p_\theta(\mathbf{x}|c_i, i = 1, ..., M) = \sum_{i=1}^{M} \log p_\theta(\mathbf{x}|c_i) - (M-1)\log p_\theta(\mathbf{x}) + \text{const.} \tag{13}$$

We can combine the compositional log-density (Equation 13) with classifier-free guidance (Equation 11) to further improve the alignment of generated samples with given concepts. The sampling gradient of the scaled log-density function is given by

$$\nabla_{\mathbf{x}} \log \tilde{p}_\theta(\mathbf{x}|c_i, i=1,...,M) = \nabla_{\mathbf{x}} \left[(w+1)\sum_{i=1}^{M} \log p_\theta(\mathbf{x}|c_i) - (Mw+M-1)\log p_\theta(\mathbf{x}) + \text{const} \right]$$
$$= (w+1)\sum_{i=1}^{M} \nabla_{\mathbf{x}} f_\theta(\mathbf{x}|c_i) - (Mw+M-1)\nabla_{\mathbf{x}} f_\theta(\mathbf{x}). \quad (14)$$

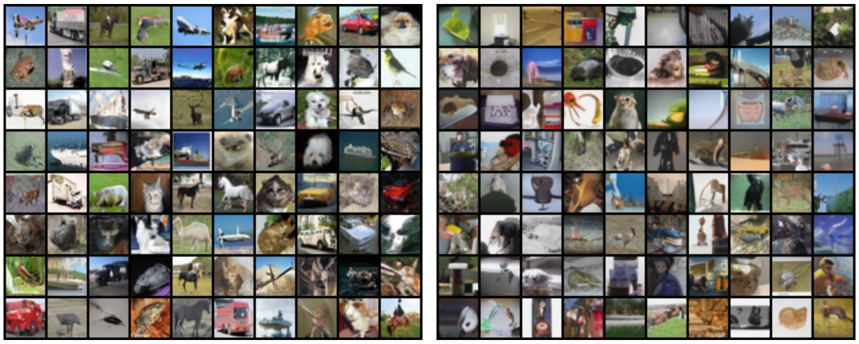

(a) CIFAR-10

(b) ImageNet (32 × 32)

Figure 1: Unconditional generated examples on CIFAR-10 and ImageNet (32 × 32) datasets.

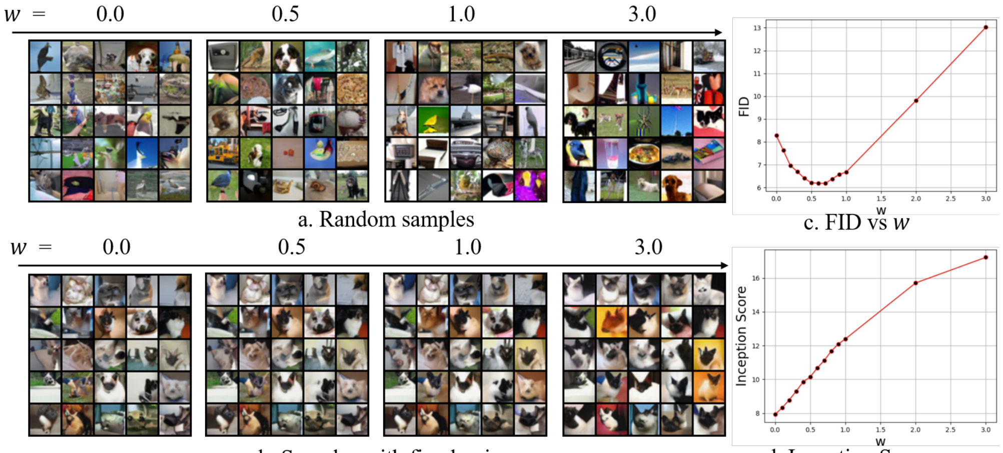

a. Random samples

c. FID vs *w*

b. Samples with fixed noise

d. Inception Score vs *w*

Figure 2: Conditional generation on ImageNet (32 × 32) dataset with a classifier-free guidance. (a) Random image samples generated with different guided weights $w = 0.0, 0.5, 1.0$ and 3.0; (b) Samples generated with a fixed noise under different guided weights. The class label is set to be the category of Siamese Cat. Sub-images presented at the same position depict samples with identical random noise and class label, differing only in their guided weights; (c) A curve of FID scores across different guided weights; (d) A curve of Inception scores across different guided weights.

4 Experiments

We evaluate the performance of our model across various scenarios. Specifically, Section 4.1 demonstrates the capacity of unconditional generation. Section 4.2 highlights the potential of our model to further optimize sampling efficiency. The focus shifts to conditional generation and classifier-free guidance in Section 4.3. Section 4.4 elucidates the power of our model in performing likelihood estimation and OOD detection, and Section 4.5 showcases compositional generation. Please refer to Appendix B for implementation details, Appendix C.1 for image inpainting with our trained models, Appendix D.3 for comparing the sampling time between our approach and other EBM

Table 1: Comparison of FID scores for unconditional generation on CIFAR-10.

Models	**FID ↓**
EBM based method	
NT-EBM (Nijkamp et al., 2022)	78.12
LP-EBM (Pang et al., 2020)	70.15
Adaptive CE (Xiao & Han, 2022)	65.01
EBM-SR (Nijkamp et al., 2019)	44.50
JEM (Grathwohl et al., 2020)	38.40
EBM-IG (Du & Mordatch, 2019)	38.20
EBM-FCE (Gao et al., 2020)	37.30
CoopVAEBM (Xie et al., 2021b)	36.20
CoopNets (Xie et al., 2018a)	33.61
Divergence Triangle (Han et al., 2020)	30.10
VARA (Grathwohl et al., 2021)	27.50
EBM-CD (Du et al., 2021)	25.10
GEBM (Arbel et al., 2021)	19.31
HAT-EBM (Hill et al., 2022)	19.30
CF-EBM (Zhao et al., 2021)	16.71
CoopFlow (Xie et al., 2022b)	15.80
CLEL-base (Lee et al., 2023)	15.27
VAEBM (Xiao et al., 2021)	12.16
DRL (Gao et al., 2021)	9.58
CLEL-large (Lee et al., 2023)	8.61
EGC (Unsupervised) (Guo et al., 2023)	5.36
CDRL (Ours)	4.31
CDRL-large (Ours)	3.68

Models	**FID ↓**
Other likelihood based method	
VAE (Kingma & Welling, 2014)	78.41
PixelCNN (Salimans et al., 2017)	65.93
PixelIQN (Ostrovski et al., 2018)	49.46
Residual Flow (Chen et al., 2019)	47.37
Glow (Kingma & Dhariwal, 2018)	45.99
DC-VAE (Parmar et al., 2021)	17.90
GAN based method	
WGAN-GP(Gulrajani et al., 2017)	36.40
SN-GAN (Miyato et al., 2018)	21.70
BigGAN (Brock et al., 2019)	14.80
StyleGAN2-DiffAugment (Zhao et al., 2020)	5.79
Diffusion-GAN (Xiao et al., 2022)	3.75
StyleGAN2-ADA (Karras et al., 2020)	2.92
Score based and Diffusion method	
NCSN (Song & Ermon, 2019)	25.32
NCSN-v2 (Song & Ermon, 2020)	10.87
NCSN++ (Song et al., 2021b)	2.20
DDPM Distillation (Luhman & Luhman, 2021)	9.36
DDPM++(VP, NLL) (Kim et al., 2021)	3.45
DDPM (Ho et al., 2020)	3.17
DDPM++(VP, FID) (Kim et al., 2021)	2.47

models, Appendix D.4 for understanding the role of EBM and initializer in the generation process and Appendix D for the ablation study. We designate our approach as "CDRL" in the following sections.

Our experiments primarily involve three datasets: (i) CIFAR-10 (Krizhevsky & Hinton, 2009) comprises images from 10 categories, with 50k training samples and 10k test samples at a resolution of 32×32 pixels. We use its training set for evaluating our model in the task of unconditional generation. (ii) ImageNet (Deng et al., 2009) contains approximately 1.28M images from 1000 categories. We use its training set for both conditional and unconditional generation, focusing on a downsampled version (32×32) of the dataset. (iii) CelebA (Liu et al., 2015) consists of around 200k human face images, each annotated with attributes. We downsample each image of the dataset to the size of 64×64 pixels and utilize the resized dataset for compositionality and image inpainting tasks.

4.1 Unconditional image generation

We first showcase our model's capabilities in unconditional image generation on CIFAR-10 and ImageNet datasets. The resolution of each image is 32×32 pixels. FID scores (Heusel et al., 2017) on these two datasets are reported in Tables 1 and 3, respectively, with generated examples displayed in Figure 1. We adopt the EBM architecture proposed in Gao et al. (2021). Additionally, we utilize a larger version called "CDRL-large", which incorporates twice as many channels in each layer. For the initializer network, we follow the structure of (Nichol & Dhariwal, 2021), utilizing a U-Net (Ronneberger et al., 2015) but halving the number of channels. Compared to Gao et al. (2021), CDRL achieves significant improvements in FID scores. Furthermore, CDRL uses the same number of noise levels (6 in total) as DRL but requires only half the MCMC steps at each noise level, reducing it from 30 to 15. This substantial reduction in computational costs is noteworthy. With the large architecture, CDRL achieves a FID score of 3.68 on CIFAR-10 and 9.35 on ImageNet (32×32). These results, to the best of our knowledge, are the state-of-the-art among existing EBM frameworks and are competitive with other strong generative model classes such as GANs and diffusion models.

4.2 Sampling efficiency

Similar to the sampling acceleration techniques employed in the diffusion model (Song et al., 2021a; Liu et al., 2022a; Lu et al., 2022), we foresee the development of post-training techniques to further accelerate CDRL sampling. Although designing an advanced MCMC sampling algorithm could be a standalone project, we present a straightforward yet effective sampling adjustment technique to demonstrate CDRL's potential in further reducing sampling time. Specifically, we propose to decrease the number of sampling steps while simultaneously adjusting the MCMC sampling step size to be inversely proportional to the square root of the number of sampling steps. As shown in Table 2, while we train CDRL with 15 MCMC steps at each noise level, we can reduce the number of MCMC steps to 8, 5, and 3 during the inference stage, without sacrificing much perceptual quality.

4.3 Conditional synthesis with classifier-free guidance

We evaluate our model for conditional generation on the ImageNet32 dataset, employing classifier-free guidance as outlined in Section 3.5. Generation results for varying guided weights w are displayed in Figure 2. As the value of w increases, the quality of samples improves, and the conditioned class features become more prominent, although diversity may decrease. This trend is also evident from the FID and Inception Score (Salimans et al., 2016) curves shown in Figures 2(c) and 2(d). While the Inception Score consistently increases (improving quality), the FID metric first drops (improving quality) and then increases (worsening quality), obtaining the optimal value of 6.18 (lowest value) at a guidance weight of 0.7. Additional image generation results can be found in Appendix C.2.

Table 2: FID for CIFAR-10 with sampling adjustment.

Models	**Number of noise level × Number of MCMC steps**	**FID ↓**
DRL (Gao et al., 2021)	$6 \times 30 = 180$	9.58
CDRL	$6 \times 15 = 90$	4.31
CDRL (step 8)	$6 \times 8 = 48$	4.58
CDRL (step 5)	$6 \times 5 = 30$	5.37
CDRL (step 3)	$6 \times 3 = 18$	9.67

Table 3: FID for ImageNet (32×32) unconditional generation.

Models	**FID ↓**
EBM-IG (Du & Mordatch, 2019)	60.23
PixelCNN (Salimans et al., 2017)	40.51
EBM-CD (Du et al., 2021)	32.48
CF-EBM (Zhao et al., 2021)	26.31
CLEL-base (Lee et al., 2023)	22.16
DRL (Gao et al., 2021)	- (not converge)
DDPM++(VP, NLL) (Kim et al., 2021)	8.42
CDRL (Ours)	9.35

4.4 Likelihood Estimation and Out-Of-Distribution Detection

A distinctive feature of the EBM is its ability to model the unnormalized log-likelihood directly using the energy function. This capability enables it to perform tasks beyond generation. In this section, we first showcase the capability of the CDRL in estimating the density of a 2D checkerboard distribution. Experimental results are presented in Figure 3, where we illustrate observed samples, the fitted density, and the generated samples at each noise level, respectively. These results confirm CDRL's ability to accurately estimate log-likelihood while simultaneously generating valid samples.

Moreover, we demonstrate CDRL's utility in out-of-distribution (OOD) detection tasks. For this endeavor, we employ the model trained on CIFAR-10 as a detector and use the energy at the lowest

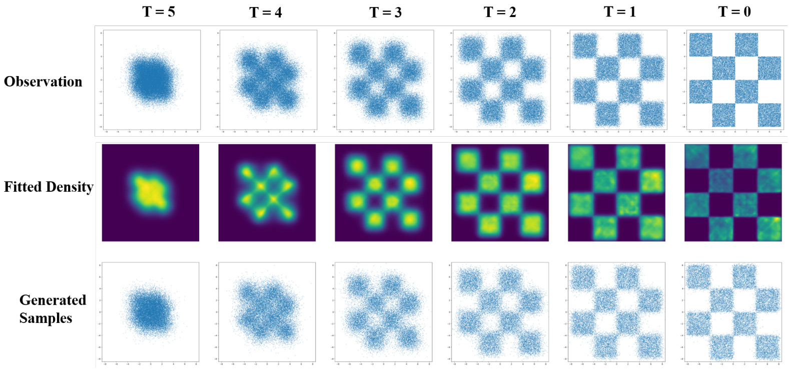

Figure 3: The results of density estimation using CDRL for a 2D checkerboard distribution. The number of noise levels in the CDRL is set to be 5. Top: observed samples at each noise level. Middle: density fitted by CDRL at each noise level. Bottom: generated samples at each noise level.

noise level to serve as the OOD prediction score. The AUROC score of our CDRL model, with CIFAR-10 interpolation, CIFAR-100, and CelebA data as OOD samples, is provided in Table 4. CDRL achieves strong results in OOD detection comparing with the baseline approaches. More results can be found in Table 8 in the appendix.

4.5 Compositionality

To evaluate the compositionality of EBMs, we conduct experiments on CelebA (64×64) datasets with *Male*, *Smile*, and *Young* as the three conditional concepts. We estimate EBMs conditional on each single concept separately, and assume simple unconditional initializer models. Classifier-free guidance is adopted when conducting compositional generation (Equation 14). Specifically, we treat images with a certain attribute value as individual classes. We randomly assign each image in a training batch to a class based on the controlled attribute value. For example, an image with Male=True and Smile=True may be assigned to class 0 if the Male attribute is picked or class 2 if the Smile attribute is picked. For the conditional network structure, we make EBM f_θ conditional on attributes c_i and use an unconditional initializer model g_ϕ to propose the initial distribution. We focus on showcasing the compositionality ability of EBM itself, although it is also possible to use a conditional initializer model similar to Section 3.5. Our results are displayed in Figure 4, with images generated at a guided weight of $w = 3.0$. More generation results with different guidance weights can be found in the Appendix C.2. Images generated with composed attributes following Equation 14 contain features of both attributes, and increasing the guided weight makes the corresponding attribute more prominent. This demonstrates CDRL's ability and the effectiveness of Equation 14.

Table 4: AUROC scores in OOD detection using CDRL and other explicit density models on CIFAR-10

	Cifar-10 interpolation	Cifar-100	CelebA
PixelCNN (Salimans et al., 2017)	0.71	0.63	-
GLOW (Kingma & Dhariwal, 2018)	0.51	0.55	0.57
NVAE (Vahdat & Kautz, 2020)	0.64	0.56	0.68
EBM-IG (Du & Mordatch, 2019)	0.70	0.50	0.70
VAEBM (Xiao et al., 2021)	0.70	0.62	0.77
EBM-CD (Du et al., 2021)	0.65	0.83	-
CLEL-Base (Lee et al., 2023)	0.72	0.72	0.77
CDRL (ours)	0.75	0.78	0.84

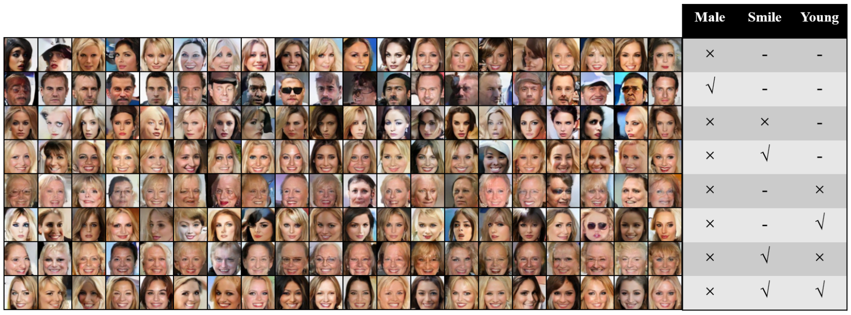

Male	Smile	Young
×	-	-
√	-	-
×	×	-
×	√	-
×	-	×
×	-	√
×	√	×
×	√	√

Figure 4: Results of attribute-compositional generation on CelebA (64×64) with guided weight $w = 3$. Left: generated samples under different attribute compositions. Right: control attributes ("$\surd$", "$\times$" and "-" indicate "True", "False" and "No Control" respectively).

5 Conclusion and Future Work

We propose CDRL, a novel energy-based generative learning framework employing cooperative diffusion recovery likelihood, which significantly enhances the generation performance of EBMs. We demonstrate that the CDRL excels in compositional generation, out-of-distribution detection, image inpainting, and compatibility with classifier-free guidance for conditional generation. One limitation is that a certain number of MCMC steps are still needed during generation. Additionally, we aim to scale our model for high-resolution image generation in the future. Our work aims to stimulate further research on developing EBMs as generative models. However, the prevalence of powerful generative models may give rise to negative social consequences, such as deepfakes, misinformation, privacy breaches, and erosion of public trust, highlighting the need for effective preventive measures.

REFERENCES

Michael Arbel, Liang Zhou, and Arthur Gretton. Generalized energy based models. In *The 9th International Conference on Learning Representations (ICLR)*, 2021.

Yoshua Bengio, Li Yao, Guillaume Alain, and Pascal Vincent. Generalized denoising auto-encoders as generative models. In *Advances in neural information processing systems (NIPS)*, 2013.

Andrew Brock, Jeff Donahue, and Karen Simonyan. Large scale GAN training for high fidelity natural image synthesis. In *The 7th International Conference on Learning Representations (ICLR)*, 2019.

Tong Che, Ruixiang Zhang, Jascha Sohl-Dickstein, Hugo Larochelle, Liam Paull, Yuan Cao, and Yoshua Bengio. Your gan is secretly an energy-based model and you should use discriminator driven latent sampling. In *Advances in Neural Information Processing Systems (NeurIPS)*, 2020.

Ricky TQ Chen, Jens Behrmann, David Duvenaud, and Jörn-Henrik Jacobsen. Residual flows for invertible generative modeling. In *Advances in Neural Information Processing Systems (NeurIPS)*, 2019.

Jiali Cui and Tian Han. Learning energy-based model via dual-mcmc teaching. In *Advances in Neural Information Processing Systems (NeurIPS)*, 2023.

Jia Deng, Wei Dong, Richard Socher, Li-Jia Li, Kai Li, and Li Fei-Fei. Imagenet: A large-scale hierarchical image database. In *Proceeding of the IEEE Conference on Computer Vision and Pattern Recognition (CVPR)*, 2009.

Prafulla Dhariwal and Alexander Quinn Nichol. Diffusion models beat gans on image synthesis. In *Advances in Neural Information Processing Systems (NeurIPS)*, 2021.

Yilun Du and Igor Mordatch. Implicit generation and generalization in energy-based models. *arXiv preprint arXiv:1903.08689*, 2019.

Yilun Du, Shuang Li, and Igor Mordatch. Compositional visual generation with energy based models. In *Advances in Neural Information Processing Systems (NeurIPS)*, 2020.

Yilun Du, Shuang Li, Joshua B. Tenenbaum, and Igor Mordatch. Improved contrastive divergence training of energy-based models. In *Proceedings of the 38th International Conference on Machine Learning (ICML)*, 2021.

Yilun Du, Conor Durkan, Robin Strudel, Joshua B Tenenbaum, Sander Dieleman, Rob Fergus, Jascha Sohl-Dickstein, Arnaud Doucet, and Will Grathwohl. Reduce, reuse, recycle: Compositional generation with energy-based diffusion models and mcmc. In *Proceedings of the 40th International Conference on Machine Learning (ICML)*, 2023.

Bradley Efron. Tweedie's formula and selection bias. *Journal of the American Statistical Association*, 106(496):1602–1614, 2011.

Patrick Esser, Robin Rombach, and Bjorn Ommer. Taming transformers for high-resolution image synthesis. In *Proceeding of the IEEE Conference on Computer Vision and Pattern Recognition (CVPR)*, 2021.

Ruiqi Gao, Yang Lu, Junpei Zhou, Song-Chun Zhu, and Ying Nian Wu. Learning generative convnets via multi-grid modeling and sampling. In *Proceeding of the IEEE Conference on Computer Vision and Pattern Recognition (CVPR)*, 2018.

Ruiqi Gao, Erik Nijkamp, Diederik P. Kingma, Zhen Xu, Andrew M Dai, and Ying Nian Wu. Flow contrastive estimation of energy-based models. In *Proceeding of the IEEE Conference on Computer Vision and Pattern Recognition (CVPR)*, 2020.

Ruiqi Gao, Yang Song, Ben Poole, Ying Nian Wu, and Diederik P. Kingma. Learning energy-based models by diffusion recovery likelihood. In *The 9th International Conference on Learning Representations (ICLR)*, 2021.

Pierre Glaser, Michael Arbel, Arnaud Doucet, and Arthur Gretton. Maximum likelihood learning of energy-based models for simulation-based inference. *arXiv preprint arXiv:2210.14756*, 2022.

Ian Goodfellow, Jean Pouget-Abadie, Mehdi Mirza, Bing Xu, David Warde-Farley, Sherjil Ozair, Aaron Courville, and Yoshua Bengio. Generative adversarial networks. *Communications of the ACM*, 63(11):139–144, 2020.

Will Grathwohl, Kuan-Chieh Wang, Jörn-Henrik Jacobsen, David Duvenaud, Mohammad Norouzi, and Kevin Swersky. Your classifier is secretly an energy based model and you should treat it like one. In *The 8th International Conference on Learning Representations (ICLR)*, 2020.

Will Sussman Grathwohl, Jacob Jin Kelly, Milad Hashemi, Mohammad Norouzi, Kevin Swersky, and David Duvenaud. No MCMC for me: Amortized sampling for fast and stable training of energy-based models. In *The 9th International Conference on Learning Representations (ICLR)*, 2021.

Ishaan Gulrajani, Faruk Ahmed, Martin Arjovsky, Vincent Dumoulin, and Aaron Courville. Improved training of wasserstein gans. In *The 6th International Conference on Learning Representations (ICLR)*, 2017.

Qiushan Guo, Chuofan Ma, Yi Jiang, Zehuan Yuan, Yizhou Yu, and Ping Luo. Egc: Image generation and classification via a diffusion energy-based model. *arXiv preprint arXiv:2304.02012*, 2023.

Tian Han, Erik Nijkamp, Xiaolin Fang, Mitch Hill, Song-Chun Zhu, and Ying Nian Wu. Divergence triangle for joint training of generator model, energy-based model, and inferential model. In *Proceeding of the IEEE Conference on Computer Vision and Pattern Recognition (CVPR)*, 2019.

Tian Han, Erik Nijkamp, Linqi Zhou, Bo Pang, Song-Chun Zhu, and Ying Nian Wu. Joint training of variational auto-encoder and latent energy-based model. In *Proceeding of the IEEE Conference on Computer Vision and Pattern Recognition (CVPR)*, 2020.

Martin Heusel, Hubert Ramsauer, Thomas Unterthiner, Bernhard Nessler, and Sepp Hochreiter. Gans trained by a two time-scale update rule converge to a local nash equilibrium. In *Advances in Neural Information Processing Systems (NeurIPS)*, 2017.

Mitch Hill, Erik Nijkamp, Jonathan Mitchell, Bo Pang, and Song-Chun Zhu. Learning probabilistic models from generator latent spaces with hat ebm. In *Advances in Neural Information Processing Systems (NeurIPS)*, 2022.

Geoffrey E Hinton. Training products of experts by minimizing contrastive divergence. *Neural computation*, 14(8):1771–1800, 2002.

Geoffrey E. Hinton. A practical guide to training restricted boltzmann machines. In *Neural Networks: Tricks of the Trade - Second Edition*, pp. 599–619. Springer, 2012.

Jonathan Ho and Tim Salimans. Classifier-free diffusion guidance. *arXiv preprint arXiv:2207.12598*, 2022.

Jonathan Ho, Ajay Jain, and Pieter Abbeel. Denoising diffusion probabilistic models. In *Advances in Neural Information Processing Systems (NeurIPS)*, 2020.

Long Jin, Justin Lazarow, and Zhuowen Tu. Introspective classification with convolutional nets. In Isabelle Guyon, Ulrike von Luxburg, Samy Bengio, Hanna M. Wallach, Rob Fergus, S. V. N. Vishwanathan, and Roman Garnett (eds.), *Advances in Neural Information Processing Systems (NIPS)*, pp. 823–833, 2017.

Tero Karras, Miika Aittala, Janne Hellsten, Samuli Laine, Jaakko Lehtinen, and Timo Aila. Training generative adversarial networks with limited data. In *Advances in Neural Information Processing Systems (NeurIPS)*, 2020.

Tero Karras, Miika Aittala, Timo Aila, and Samuli Laine. Elucidating the design space of diffusion-based generative models. In *Advances in Neural Information Processing Systems (NeurIPS)*, 2022.

Dongjun Kim, Seungjae Shin, Kyungwoo Song, Wanmo Kang, and Il-Chul Moon. Soft truncation: A universal training technique of score-based diffusion model for high precision score estimation. In *Proceedings of the 38th International Conference on Machine Learning (ICML)*, 2021.

Taesup Kim and Yoshua Bengio. Deep directed generative models with energy-based probability estimation. *arXiv preprint arXiv:1606.03439*, 2016.

Diederik P. Kingma and Jimmy Ba. Adam: A method for stochastic optimization. In *The 3rd International Conference on Learning Representations (ICLR)*, 2015.

Diederik P. Kingma and Prafulla Dhariwal. Glow: Generative flow with invertible 1x1 convolutions. In *Advances in Neural Information Processing Systems (NeurIPS)*, 2018.

Diederik P. Kingma and Max Welling. Auto-encoding variational bayes. In *The 2nd International Conference on Learning Representations (ICLR)*, 2014.

Diederik P. Kingma, Tim Salimans, Ben Poole, and Jonathan Ho. Variational diffusion models. In *Advances in neural information processing systems (NeurIPS)*, 2021.

Lingkai Kong, Jiaming Cui, Yuchen Zhuang, Rui Feng, B. Aditya Prakash, and Chao Zhang. End-to-end stochastic optimization with energy-based model. In *Advances in Neural Information Processing Systems (NeurIPS)*, 2022.

Alex Krizhevsky and Geoffrey Hinton. Learning multiple layers of features from tiny images. 2009.

Rithesh Kumar, Sherjil Ozair, Anirudh Goyal, Aaron Courville, and Yoshua Bengio. Maximum entropy generators for energy-based models. *arXiv preprint arXiv:1901.08508*, 2019.

Justin Lazarow, Long Jin, and Zhuowen Tu. Introspective neural networks for generative modeling. In *IEEE International Conference on Computer Vision (ICCV)*, pp. 2793–2802, 2017.

Yann LeCun, Sumit Chopra, Raia Hadsell, M Ranzato, and Fujie Huang. A tutorial on energy-based learning. *Predicting structured data*, 1(0), 2006.

Hankook Lee, Jongheon Jeong, Sejun Park, and Jinwoo Shin. Guiding energy-based models via contrastive latent variables. In *The 11th International Conference on Learning Representations (ICLR)*, 2023.

Kwonjoon Lee, Weijian Xu, Fan Fan, and Zhuowen Tu. Wasserstein introspective neural networks. In *IEEE Conference on Computer Vision and Pattern Recognition (CVPR)*, pp. 3702–3711, 2018.

Yaron Lipman, Ricky TQ Chen, Heli Ben-Hamu, Maximilian Nickel, and Matt Le. Flow matching for generative modeling. *arXiv preprint arXiv:2210.02747*, 2022.

Luping Liu, Yi Ren, Zhijie Lin, and Zhou Zhao. Pseudo numerical methods for diffusion models on manifolds. In *The 10th International Conference on Learning Representations (ICLR)*, 2022a.

Meng Liu, Keqiang Yan, Bora Oztekin, and Shuiwang Ji. Graphebm: Molecular graph generation with energy-based models. In *ICLR workshop on Energy-Based Model*, 2021.

Weitang Liu, Xiaoyun Wang, John D. Owens, and Yixuan Li. Energy-based out-of-distribution detection. In *Advances in Neural Information Processing Systems (NeurIPS)*, 2020.

Xingchao Liu, Chengyue Gong, and Qiang Liu. Flow straight and fast: Learning to generate and transfer data with rectified flow. *arXiv preprint arXiv:2209.03003*, 2022b.

Ziwei Liu, Ping Luo, Xiaogang Wang, and Xiaoou Tang. Deep learning face attributes in the wild. In *Proceedings of the International Conference on Computer Vision (ICCV)*, 2015.

Ilya Loshchilov and Frank Hutter. Decoupled weight decay regularization. In *The 7th International Conference on Learning Representations (ICLR)*, 2019.

Cheng Lu, Yuhao Zhou, Fan Bao, Jianfei Chen, Chongxuan Li, and Jun Zhu. Dpm-solver: A fast ODE solver for diffusion probabilistic model sampling in around 10 steps. In *Advances in Neural Information Processing Systems (NeurIPS)*, 2022.

Eric Luhman and Troy Luhman. Knowledge distillation in iterative generative models for improved sampling speed. *arXiv preprint arXiv:2101.02388*, 2021.

Takeru Miyato, Toshiki Kataoka, Masanori Koyama, and Yuichi Yoshida. Spectral normalization for generative adversarial networks. In *The 6th International Conference on Learning Representations (ICLR)*, 2018.

Jiquan Ngiam, Zhenghao Chen, Pang Wei Koh, and Andrew Y. Ng. Learning deep energy models. In *Proceedings of the 28th international conference on machine learning (ICML)*, 2011.

Alexander Quinn Nichol and Prafulla Dhariwal. Improved denoising diffusion probabilistic models. In *Proceedings of the 38th International Conference on Machine Learning (ICML)*, 2021.

Erik Nijkamp, Mitch Hill, Song-Chun Zhu, and Ying Nian Wu. Learning non-convergent non-persistent short-run MCMC toward energy-based model. In *Advances in Neural Information Processing Systems (NeurIPS)*, 2019.

Erik Nijkamp, Ruiqi Gao, Pavel Sountsov, Srinivas Vasudevan, Bo Pang, Song-Chun Zhu, and Ying Nian Wu. Learning energy-based model with flow-based backbone by neural transport mcmc. In *The 9th International Conference on Learning Representations (ICLR)*, 2022.

Georg Ostrovski, Will Dabney, and Rémi Munos. Autoregressive quantile networks for generative modeling. In *Proceedings of the 35th International Conference on Machine Learning (ICML)*, 2018.

Bo Pang, Tian Han, Erik Nijkamp, Song-Chun Zhu, and Ying Nian Wu. Learning latent space energy-based prior model. In *Advances in Neural Information Processing Systems (NeurIPS)*, 2020.

Gaurav Parmar, Dacheng Li, Kwonjoon Lee, and Zhuowen Tu. Dual contradistinctive generative autoencoder. In *Proceeding of the IEEE Conference on Computer Vision and Pattern Recognition (CVPR)*, 2021.

Aditya Ramesh, Prafulla Dhariwal, Alex Nichol, Casey Chu, and Mark Chen. Hierarchical text-conditional image generation with clip latents. *arXiv preprint arXiv:2204.06125*, 2022.

Herbert E Robbins. *An empirical Bayes approach to statistics*. Springer, 1992.

Robin Rombach, Andreas Blattmann, Dominik Lorenz, Patrick Esser, and Björn Ommer. High-resolution image synthesis with latent diffusion models. In *Proceeding of the IEEE Conference on Computer Vision and Pattern Recognition (CVPR)*, 2022.

Olaf Ronneberger, Philipp Fischer, and Thomas Brox. U-net: Convolutional networks for biomedical image segmentation. In *Medical Image Computing and Computer-Assisted Intervention (MICCAI)*, 2015.

Chitwan Saharia, William Chan, Saurabh Saxena, Lala Li, Jay Whang, Emily L. Denton, Seyed Kamyar Seyed Ghasemipour, Raphael Gontijo Lopes, Burcu Karagol Ayan, Tim Salimans, Jonathan Ho, David J. Fleet, and Mohammad Norouzi. Photorealistic text-to-image diffusion models with deep language understanding. In *Advances in Neural Information Processing Systems (NeurIPS)*, 2022.

Tim Salimans and Jonathan Ho. Should ebms model the energy or the score? In *ICLR workshop on Energy-Based Model*, 2021.

Tim Salimans and Jonathan Ho. Progressive distillation for fast sampling of diffusion models. In *The 10th International Conference on Learning Representations (ICLR)*, 2022.

Tim Salimans, Ian J. Goodfellow, Wojciech Zaremba, Vicki Cheung, Alec Radford, and Xi Chen. Improved techniques for training gans. In *Advances in Neural Information Processing Systems (NIPS)*, 2016.

Tim Salimans, Andrej Karpathy, Xi Chen, and Diederik P. Kingma. Pixelcnn++: Improving the pixelcnn with discretized logistic mixture likelihood and other modifications. In *The 5th International Conference on Learning Representations (ICLR)*, 2017.

Jascha Sohl-Dickstein, Eric A. Weiss, Niru Maheswaranathan, and Surya Ganguli. Deep unsupervised learning using nonequilibrium thermodynamics. In *Proceedings of the 32nd International Conference on Machine Learning (ICML)*, 2015.

Jiaming Song, Chenlin Meng, and Stefano Ermon. Denoising diffusion implicit models. In *The 9th International Conference on Learning Representations (ICLR)*, 2021a.

Yang Song and Stefano Ermon. Generative modeling by estimating gradients of the data distribution. In *Advances in Neural Information Processing Systems (NeurIPS)*, 2019.

Yang Song and Stefano Ermon. Improved techniques for training score-based generative models. In *Advances in Neural Information Processing Systems (NeurIPS)*, 2020.

Yang Song, Jascha Sohl-Dickstein, Diederik P. Kingma, Abhishek Kumar, Stefano Ermon, and Ben Poole. Score-based generative modeling through stochastic differential equations. In *The 9th International Conference on Learning Representations (ICLR)*, 2021b.

Arash Vahdat and Jan Kautz. NVAE: A deep hierarchical variational autoencoder. In *Advances in Neural Information Processing Systems (NeurIPS)*, 2020.

Zhisheng Xiao and Tian Han. Adaptive multi-stage density ratio estimation for learning latent space energy-based model. In *Advances in Neural Information Processing Systems (NeurIPS)*, 2022.

Zhisheng Xiao, Karsten Kreis, Jan Kautz, and Arash Vahdat. Vaebm: A symbiosis between variational autoencoders and energy-based models. In *The 9th International Conference on Learning Representations (ICLR)*, 2021.

Zhisheng Xiao, Karsten Kreis, and Arash Vahdat. Tackling the generative learning trilemma with denoising diffusion gans. In *The 9th International Conference on Learning Representations (ICLR)*, 2022.

Jianwen Xie, Yang Lu, Song-Chun Zhu, and Ying Nian Wu. A theory of generative convnet. In *Proceedings of the 33nd International Conference on Machine Learning (ICML)*, 2016.

Jianwen Xie, Yang Lu, Ruiqi Gao, Song-Chun Zhu, and Ying Nian Wu. Cooperative training of descriptor and generator networks. *IEEE Transactions on Pattern Analysis and Machine intelligence (TPAMI)*, 42(1):27–45, 2018a.

Jianwen Xie, Zilong Zheng, Ruiqi Gao, Wenguan Wang, Song-Chun Zhu, and Ying Nian Wu. Learning descriptor networks for 3d shape synthesis and analysis. In *Proceeding of the IEEE Conference on Computer Vision and Pattern Recognitio (CVPR)*, 2018b.

Jianwen Xie, Yang Lu, Ruiqi Gao, Song-Chun Zhu, and Ying Nian Wu. Cooperative training of descriptor and generator networks. *IEEE Transactions on Pattern Analysis and Machine Intelligence (TPAMI)*, 42(1):27–45, 2020.

Jianwen Xie, Yifei Xu, Zilong Zheng, Song-Chun Zhu, and Ying Nian Wu. Generative pointnet: Deep energy-based learning on unordered point sets for 3d generation, reconstruction and classification. In *Proceeding of the IEEE Conference on Computer Vision and Pattern Recognition (CVPR)*, 2021a.

Jianwen Xie, Zilong Zheng, and Ping Li. Learning energy-based model with variational auto-encoder as amortized sampler. In *Proceeding of the 35th AAAI Conference on Artificial Intelligence (AAAI)*, 2021b.

Jianwen Xie, Song-Chun Zhu, and Ying Nian Wu. Learning energy-based spatial-temporal generative convnets for dynamic patterns. *IEEE Transactions on Pattern Analysis and Machine Intelligence (TPAMI)*, 43(2):516–531, 2021c.

Jianwen Xie, Zilong Zheng, Xiaolin Fang, Song-Chun Zhu, and Ying Nian Wu. Cooperative training of fast thinking initializer and slow thinking solver for conditional learning. *EEE Transactions on Pattern Analysis and Machine Intelligence (TPAMI)*, 44(8):3957–3973, 2022a.

Jianwen Xie, Yaxuan Zhu, Jun Li, and Ping Li. A tale of two flows: Cooperative learning of langevin flow and normalizing flow toward energy-based model. In *The 10th International Conference on Learning Representations (ICLR)*, 2022b.

Xuwang Yin, Shiying Li, and Gustavo K Rohde. Learning energy-based models with adversarial training. In *The European Conference on Computer Vision (ECCV)*, 2022.

Sangwoong Yoon, Young-Uk Jin, Yung-Kyun Noh, and Frank C Park. Energy-based models for anomaly detection: A manifold diffusion recovery approach. *arXiv preprint arXiv:2310.18677*, 2023.

Peiyu Yu, Yaxuan Zhu, Sirui Xie, Xiaojian Shawn Ma, Ruiqi Gao, Song-Chun Zhu, and Ying Nian Wu. Learning energy-based prior model with diffusion-amortized mcmc. In *Advances in Neural Information Processing Systems (NeurIPS)*, 2023.

Jing Zhang, Jianwen Xie, Nick Barnes, and Ping Li. An energy-based prior for generative saliency. *IEEE Transactions on Pattern Analysis and Machine Intelligence (TPAMI)*, 45(11):13100–13116, 2023.

Shengyu Zhao, Zhijian Liu, Ji Lin, Jun-Yan Zhu, and Song Han. Differentiable augmentation for data-efficient GAN training. In *Advances in Neural Information Processing Systems (NeurIPS)*, 2020.

Yang Zhao, Jianwen Xie, and Ping Li. Learning energy-based generative models via coarse-to-fine expanding and sampling. In *The 9th International Conference on Learning Representations (ICLR)*, 2021.

Song-Chun Zhu, Ying Nian Wu, and David Mumford. Filters, random fields and maximum entropy (frame): Towards a unified theory for texture modeling. *International Journal of Computer Vision (IJCV)*, 27:107–126, 1998.

Yaxuan Zhu, Jianwen Xie, and Ping Li. Likelihood-based generative radiance field with latent space energy-based model for 3d-aware disentangled image representation. In *International Conference on Artificial Intelligence and Statistics (AISTATS)*, 2023.

APPENDICES

A RELATED WORK

Energy-Based Learning Energy-based models (EBMs) (Zhu et al., 1998; LeCun et al., 2006; Ngiam et al., 2011; Hinton, 2012; Xie et al., 2016) define unnormalized probabilistic distributions and are typically trained through maximum likelihood estimation. Methods such as contrastive divergence (Hinton, 2002; Du et al., 2021), persistent chain (Xie et al., 2016), replay buffer (Du & Mordatch, 2019) or short-run MCMC sampling (Nijkamp et al., 2019) approximate the analytically intractable learning gradient. To scale up and stabilize EBM training for high-fidelity data generation, strategies like multi-grid sampling (Gao et al., 2018), progressive training (Zhao et al., 2021), and diffusion (Gao et al., 2021) have been adopted. EBMs have also been connected to other models, such as adversarial training (Arbel et al., 2021; Che et al., 2020), variational autoencoders (Xiao et al., 2021), contrastive guidance (Lee et al., 2023), introspective learning (Lazarow et al., 2017; Jin et al., 2017; Lee et al., 2018), and noise contrastive estimation (Gao et al., 2020). To alleviate MCMC burden, various methods have been proposed, including amortizing MCMC sampling with learned networks (Kim & Bengio, 2016; Xie et al., 2018a; Kumar et al., 2019; Xiao et al., 2021; Han et al., 2019; Grathwohl et al., 2021). Among them, cooperative networks (CoopNets) (Xie et al., 2018a) jointly train a top-down generator and an EBM via MCMC teaching, using the generator as a fast initializer for Langevin sampling. CoopNets variants have also been studied in Xie et al. (2021b; 2022b). Our work improves the recovery likelihood learning algorithm of EBMs (Gao et al., 2021) by learning a fast MCMC initializer for EBM sampling, leveraging the cooperative learning scheme (Xie et al., 2020). Compared to Xie et al. (2020) that applied cooperative training to an initializer and an EBM for the *marginal* distribution of the clean data, our approach only requires learning *conditional* initializers and sampling from *conditional* EBMs, which are much more tractable than their marginal counterparts. It is worth noting that Xie et al. (2022a) have investigated conditional cooperative learning, wherein a conditional initializer and a conditional EBM are trained through MCMC teaching. In contrast, our CDRL trains and samples from a sequence of conditional EBMs and conditional initializers on increasingly noisy versions of a dataset for denoising diffusion generation.

Denoising Diffusion Model Diffusion models, initially introduced by Sohl-Dickstein et al. (2015) and further developed in subsequent works such as Song & Ermon (2020); Ho et al. (2020), generate samples by progressively denoising them from a high noise level to clean data. These models have demonstrated significant success in generating high-quality samples from complex distributions, owing to a range of architectural and algorithmic innovations (Ho et al., 2020; Song et al., 2021a; Kim et al., 2021; Song et al., 2021b; Dhariwal & Nichol, 2021; Karras et al., 2022; Ho & Salimans, 2022). Notably, Dhariwal & Nichol (2021) emphasize that the generative performance of diffusion models can be enhanced with the aid of a classifier, while Ho & Salimans (2022) further demonstrate that this guided scoring can be estimated by the differential scores of a conditional model versus an unconditional model. Enhancements in sampling speed have been realized through distillation techniques (Salimans & Ho, 2022) and the development of fast SDE/ODE samplers (Song et al., 2021a; Karras et al., 2022; Lu et al., 2022). Recent advancements (Rombach et al., 2022; Saharia et al., 2022; Ramesh et al., 2022) have successfully applied conditional diffusion models to the task of text-to-image generation, achieving significant breakthroughs.

EBM shares a close relationship with diffusion models, as both frameworks can provide a score to guide the generation process, whether through Langevin dynamics or SDE/ODE solvers. As Salimans & Ho (2021) discuss, the distinction between these two models lies in their implementation approaches: EBMs model the log-likelihood directly, while diffusion models focus on the gradient of the log-likelihood. This distinction brings advantages to EBMs, such as their compatibility with advanced sampling techniques (Du et al., 2023), potential conversion into classifiers (Guo et al., 2023), and capability to detect abnormal samples through estimated likelihood (Grathwohl et al., 2020; Liu et al., 2020).

The primary focus of this work is to advance the development of EBMs. Our approach connects with diffusion models (Ho et al., 2020; Xiao et al., 2022) by training a sequence of EBMs and MCMC initializers to reverse the diffusion process. In contrast to Ho et al. (2020), our framework employs more expressive conditional EBMs instead of normal distributions to represent the denoising distribution. Additionally, Xiao et al. (2022) also suggest multimodal distributions, trained by generative adversarial networks (Goodfellow et al., 2020), for the reverse process.

B Training Details

B.1 Network Architectures

We adopt the EBM architecture from (Gao et al., 2021), starting with a 3×3 convolution layer with 128 channels (The number of channels is doubled to 256 in the CDRL-large configuration). We use several downsample blocks for resolution adjustments, each containing multiple residual blocks. All downsampling blocks, except the last one, include a 2×2 average pooling layer. Spectral normalization is applied to all convolution layers for stability, while ReLU activation is applied to the final feature map. The energy output is obtained by summing the values over spatial and channel dimensions. The architectures of EBM building blocks are shown in Table 5, and the hyperparameters of network architecture are displayed in Table 6.

For the initializer network, we follow (Nichol & Dhariwal, 2021) to utilize a U-Net (Ronneberger et al., 2015) while halving the number of channels. This reduction effectively decreases the size of the initializer model. For an image with a resolution of 32×32 pixels, we have feature map resolutions of 32×32, 16×16, and 4×4. When dealing with 64×64 images, we include an additional feature map resolution of 64×64. All feature map channel numbers are set to 64, with attention applied to resolutions of 16×16 and 8×8. Our initializer directly predicts the noised image $\tilde{\mathbf{y}}_t$ at each noise level t, while the DDPM in (Ho et al., 2020) predicts the total injected noise ϵ.

For the class-conditioned generation task, we map class labels to one-hot vectors and use a fully-connected layer to map these vectors to class embedding vectors with the same dimensions as time embedding vectors. The class embedding is then added to the time embedding. We set the time embedding dimension to 512 for EBM and 256 for the initializer in the CDRL setting. In the

CDRL-large setting, the time embedding dimension increases to 1024 for EBM, while the one in the initializer remains unchanged.

Table 5: Building blocks of the EBM in CDRL.

(a) ResBlock

leakyReLU, 3 × 3 Conv2D
+ Dense(leakyReLU(temb))
leakyReLU, 3 × 3 Conv2D
+ Input

(b) Downsample Block

N ResBlocks
Downsample 2 × 2

(c) Time Embedding

Sinusoidal Embedding
Dense, leakyReLU
Dense

Table 6: Hyperparameters for EBM architectures in different settings.

Model	# of Downsample Blocks	N (# of Resblocks in Downsample Block)	# of channels in each resolution
CDRL (32×32)	4	8	(128, 256, 256, 256)
CDRL-large (32×32)	4	8	(256, 512, 512, 512)
Compositionality Exp.	5	2	(128, 256, 256, 256, 256)
Inpainting Exp.	5	8	(128, 256, 256, 256, 256)

B.2 HYPERPARAMETERS

We set the learning rate of EBM to be $\eta_\theta = 1e-4$ and the learning rate of initializer to be $\eta_\phi = 1e-5$. We use linear warm up for both EBM and initializer and let the initializer to start earlier than EBM. More specifically, given training iteration iter, we have:

$$\eta_\theta = \min(1.0, \frac{\text{iter}}{10000}) \times 1e-4$$
$$\eta_\phi = \min(1.0, \frac{\text{iter}+500}{10000}) \times 1e-5 \tag{15}$$

We use the Adam optimizer Kingma & Ba (2015); Loshchilov & Hutter (2019) to train both the EBM and the initializer, with $\beta = (0.9, 0.999)$ and a weight decay equal to 0.0. We also apply exponential moving average with a decay rate equal to 0.9999 to both the EBM and the initializer. Training is conducted across 8 Nvidia A100 GPUs, typically requiring approximately 400k iterations, which spans approximately 6 days.

Following (Gao et al., 2021), we use a re-parameterization trick to calculate the energy term. Our EBM is constructed across noise levels $t = 0, 1, 2, 3, 4, 5$ and we assume the distribution at noise level $t = 6$ is a simple Normal distribution during sampling. Given $\mathbf{y}_t$ under noise level t, suppose we denote the output of the EBM network as $\hat{f}_\theta(\mathbf{y}_t, t)$, then the true energy term is given by $f_\theta(\mathbf{y}_t, t) = \frac{\hat{f}_\theta(\mathbf{y}_t,t)}{s_t^2}$, where s_t is the Langevin step size at noise level t. In other words, we parameterize the energy as the product of the EBM network output and a noise-level dependent coefficient, setting this coefficient equal to the square of the Langevin step size. We use 15 steps of Langevin updates at each noise level, with the Langevin step size at noise level t given by

$$s_t^2 = 0.054 \times \bar{\sigma}_t \times \sigma_{t+1}^2, \tag{16}$$

where σ_{t+1}^2 is the variance of the added noise at noise level $t+1$ and $\bar{\sigma}_t$ is the standard deviation of the accumulative noise at noise level t. During the generation process, we begin by randomly sampling $\mathbf{x}_6 \sim \mathcal{N}(0, \boldsymbol{I})$ and perform denoising using both the initializer and the Langevin Dynamics of the EBM, which follows Algorithm 2. After obtaining samples $\mathbf{x}_0$ at the lowest noise level $t = 0$, we perform an additional denoising step, where we disable the noise term in the Langevin step, to further enhance its quality. More specifically, we follow Tweedie's formula (Efron, 2011; Robbins, 1992), which states that given $\mathbf{x} \sim p_{data}(\mathbf{x})$ and a noisy version image $\mathbf{x}'$ with conditional distribution $p(\mathbf{x}'|\mathbf{x}) = \mathcal{N}(\mathbf{x}, \sigma^2 \boldsymbol{I})$, the marginal distribution can be defined as $p(\mathbf{x}') = \int p_{data}(\mathbf{x})p(\mathbf{x}'|\mathbf{x})d\mathbf{x}$. Consequently, we have

$$\mathbb{E}(\mathbf{x}|\mathbf{x}') = \mathbf{x}' + \sigma^2 \nabla_{\mathbf{x}'} \log p(\mathbf{x}'). \tag{17}$$

In our case, we have $p(\mathbf{x}_t|\bar{\alpha}_t\mathbf{x}_0) = \mathcal{N}(\bar{\alpha}_t\mathbf{x}_0, \bar{\sigma}_t^2 \boldsymbol{I})$ and we use EBM to model the marginal distribution of $\mathbf{x}_t$ as $p_{\theta,t}(\mathbf{x}_t)$, thus

$$\begin{aligned} \mathbb{E}(\bar{\alpha}_t\mathbf{x}_0|\mathbf{x}_t) &= \mathbf{x}_t + \bar{\sigma}_t^2 \nabla_{\mathbf{x}_t} \log p_{\theta,t}(\mathbf{x}_t), \\ \mathbb{E}(\mathbf{x}_0|\mathbf{x}_t) &= \frac{\mathbf{x}_t + \bar{\sigma}_t^2 \nabla_{\mathbf{x}_t} \log p_{\theta,t}(\mathbf{x}_t)}{\bar{\alpha}_t}. \end{aligned} \tag{18}$$

Suppose the samples we obtain at $t = 0$ are denoted as $\mathbf{x}_0$. These samples actually contains a small amount of noise corresponding to $\bar{\alpha}_0$, thus, we may use Equation 18 to further denoise them. In practice, we find that enlarging the denoising step by multiplying the gradient term $\nabla_{\mathbf{x}_t} \log p_{\theta,t}(\mathbf{x}_t)$ by a coefficient larger than 1.0 yields better results. We set this coefficient to be 2.0 in our experiments.

B.3 Noise Schedule and Conditioning Input

We improve upon the noise schedule and the conditioning input of DRL (Gao et al., 2021). Let $\lambda_t = \log \frac{\bar{\alpha}_t^2}{\bar{\sigma}_t^2}$ represent the logarithm of signal-to-noise ratio at noise level t. Inspired by (Kingma et al., 2021), we utilize λ_t as the conditioning input of the noise level and feed it to the networks f_θ and $\boldsymbol{g}_\phi$ instead of directly using t.

For the noise schedule, we keep the design of using 6 noise levels as in DRL. Inspired by (Nichol & Dhariwal, 2021), we construct a cosine schedule such that λ_t is defined as $\lambda_t = -2\log(\tan(at + b))$, where a and b are calculated from the maximum log SNR (denoted as $\lambda_{\max}$) and the minimum log SNR (denoted as $\lambda_{\min}$) using

$$b = \arctan(\exp(-0.5\lambda_{\max})), \tag{19}$$

$$a = \arctan(\exp(-0.5\lambda_{\min})) - b. \tag{20}$$

We set $\lambda_{\max} = 9.8$ and $\lambda_{\min} = -5.1$ to correspond with the standard deviation $\bar{\alpha}_t$ of the accumulative noise in the original Recovery Likelihood model (T6 setting) at the highest and lowest noise levels. Figure 5 illustrates the noise schedule of DRL alongside our proposed schedule. In contrast to the DRL's original schedule, our proposed schedule places more emphasis on regions with lower signal-to-noise ratios, which are vital for generating low-frequency, high-level concepts in samples.

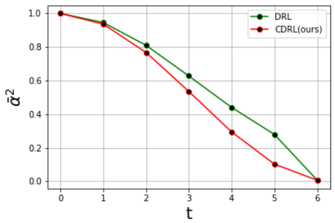

Figure 5: Noise schedule. The green line represents the noise schedule used by DRL (Gao et al., 2021) while the red line depicts the noise schedule employed by our CDRL.

B.4 Illustration of the CDRL Framework

Figure 6 illustrates the training and sampling processes of the CDRL framework, providing a comprehensive overview of the model.

C More Experimental Results

C.1 Image Inpainting

We demonstrate the inpainting ability of our learned model on the 64×64 CelebA dataset. Each image is masked, and our model is tasked with filling in the masked area. We gradually add noise to the masked image up to the final noise level, allowing the model to denoise the image progressively, similar to the standard generation process. During inpainting, only the masked area is updated, while the values in the unmasked area are retained. This is achieved by resetting the unmasked area values to the current noisy version after each Langevin update step of the EBM or initializer proposal step. Our results, depicted in Figure 7, include two types of masking: a regular square mask and an

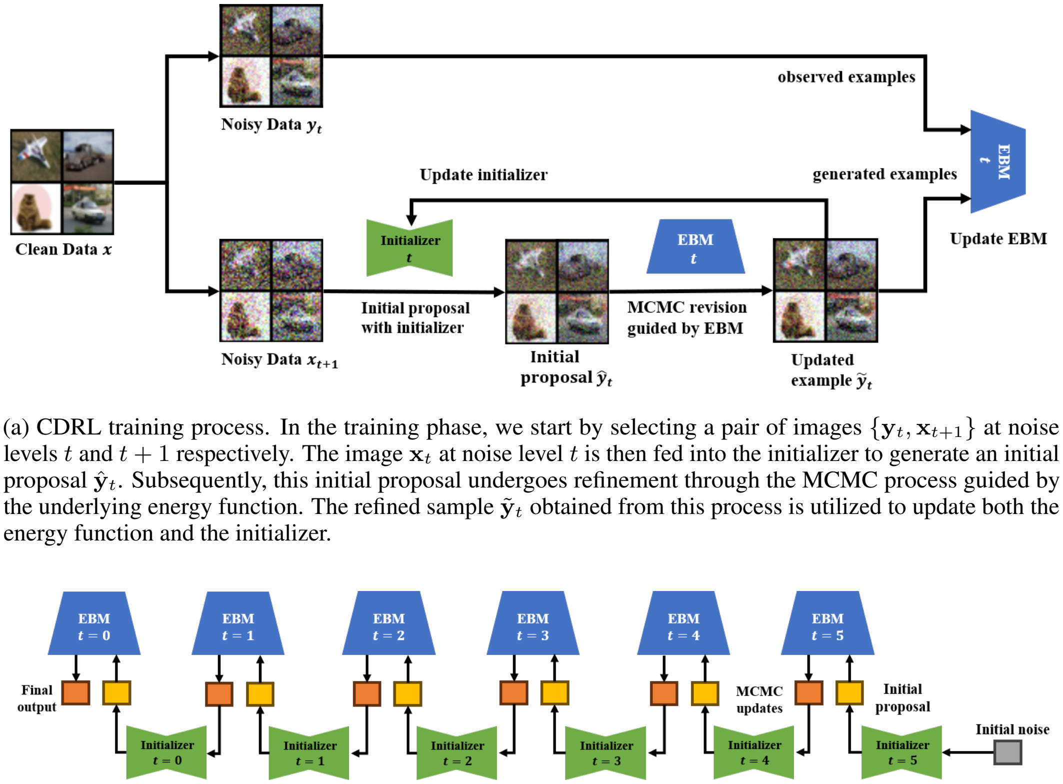

(a) CDRL training process. In the training phase, we start by selecting a pair of images $\{\mathbf{y}_t, \mathbf{x}_{t+1}\}$ at noise levels t and $t+1$ respectively. The image $\mathbf{x}_t$ at noise level t is then fed into the initializer to generate an initial proposal $\hat{\mathbf{y}}_t$. Subsequently, this initial proposal undergoes refinement through the MCMC process guided by the underlying energy function. The refined sample $\tilde{\mathbf{y}}_t$ obtained from this process is utilized to update both the energy function and the initializer.

(b) CDRL Sampling process. The sampling phase starts from Gaussian noise. Starting from the highest noise level, an initial proposal is generated by the initializer that corresponds to that noise level. Subsequently, the samples undergo refinement through MCMC sampling. This denoising process is iteratively repeated to push the noisy image towards lower noise levels until the lowest noise level $t = 0$ is reached.

Figure 6: Illustration of the Cooperative Diffusion Recovery Likelihood (CDRL) framework

irregularly shaped mask. In Figure 7, the first two columns respectively display the original images and the masked images, while the other columns show the corresponding inpainting results. CDRL successfully inpaints valid and diverse values in the masked area, producing inpainted results that differ from the observations. This suggest that CDRL does not merely memorize data because it fills novel and meaningful content into unobserved areas based on the statistical features of the dataset.

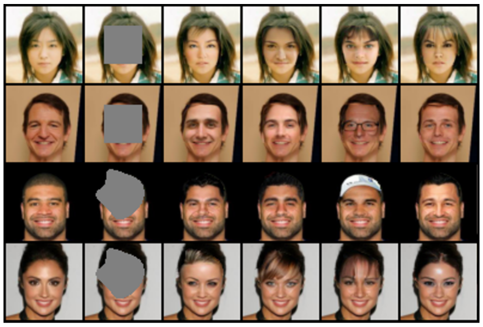

Figure 7: Results of Image inpainting on CelebA (64 × 64) dataset. The first two rows utilize square masks, while the last two rows use irregular masks. The first column displays the original images. The second column shows the masked images. Columns three to six display inpainted images using different initialization noises.

C.2 Image Generation

In this section we present additional generation results. Figure 10 showcases more compositionality results with varying guidance weights on the CelebA 64×64 dataset. Here, $w = 0.0$ corresponds to the original setting without guidance in Equation 13 in the main paper. In Figure 11, 12, 13, 14 and 15, we provide more results for conditional generation on ImageNet32 (32×32) with different guidance weights. Specifically, Figure 11 showcases random samples, while each figure in Figures 12, 13, 14 and 15 contains samples from a specific class under different guidance weights w.

C.3 Generating High-Resolution Images

The recent trend in generative modeling of high-resolution images involves either utilizing the latent space of a VAE, as demonstrated in latent diffusion (Rombach et al., 2022), or initially generating a low-resolution image and then gradually expanding it, as exemplified by techniques like Imagen (Saharia et al., 2022). This process often reduce the modeled space to dimensions such as 32×32 or 64×64, which aligns with the resolutions that we used in our experiments in the main text. Here, we conduct additional experiments by learning CDRL following Rombach et al. (2022). We conduct experiments on the CelebA-HQ dataset, and the generated samples are shown in Figure 8. Additionally, we report the FIDs in Table 7.

Table 7: Comparison of FIDs on the CelebA-HQ (256 x 256) dataset

Model	**FID score**
GLOW (Kingma & Dhariwal, 2018)	68.93
VAEBM (Xiao et al., 2021)	20.38
ATEBM (Yin et al., 2022)	17.31
VQGAN+Transformer (Esser et al., 2021)	10.2
LDM (Rombach et al., 2022)	5.11
CDRL(ours)	10.74

C.4 Out-of-Distribution Detection

We present the results for the out-of-distribution (OOD) detection task on additional datasets, along with incorporating more recent baselines. The comprehensive results are summarized in Table 8.

Table 8: Comparison of AUROC scores in OOD detection on CIFAR-10 dataset. The AUROC score for DRL (Gao et al., 2021) is reported by Yoon et al. (2023). For EBM-CD (Du et al., 2021), we present two sets of performance results from different sources: one from Du et al. (2021) and the other from a recent study (Yoon et al., 2023). We include both sets of results, with scores from Yoon et al. (2023) presented in brackets for comparison.

	Cifar-10 interpolation	**Cifar-100**	**CelebA**	**SVHN**	**Texture**
PixelCNN(Salimans et al., 2017)	0.71	0.63	-	0.32	0.33
GLOW (Kingma & Dhariwal, 2018)	0.51	0.55	0.57	0.24	0.27
NVAE (Vahdat & Kautz, 2020)	0.64	0.56	0.68	0.42	-
EBM-IG (Du & Mordatch, 2019)	0.70	0.50	0.70	0.63	0.48
VAEBM (Xiao et al., 2021)	0.70	0.62	0.77	0.83	-
EBM-CD (Du et al., 2021)	0.65 (-)	0.83 (0.53)	- (0.54)	0.91 (0.78)	0.88 (0.73)
CLEL (Lee et al., 2023)	0.72	0.72	0.77	0.98	0.94
DRL (Gao et al., 2021)	-	0.44	0.64	0.88	0.45
MPDR-S(Yoon et al., 2023)	-	0.56	0.73	0.99	0.66
MPDR_R(Yoon et al., 2023)	-	0.64	0.83	0.98	0.80
CDRL	0.75	0.78	0.84	0.82	0.65

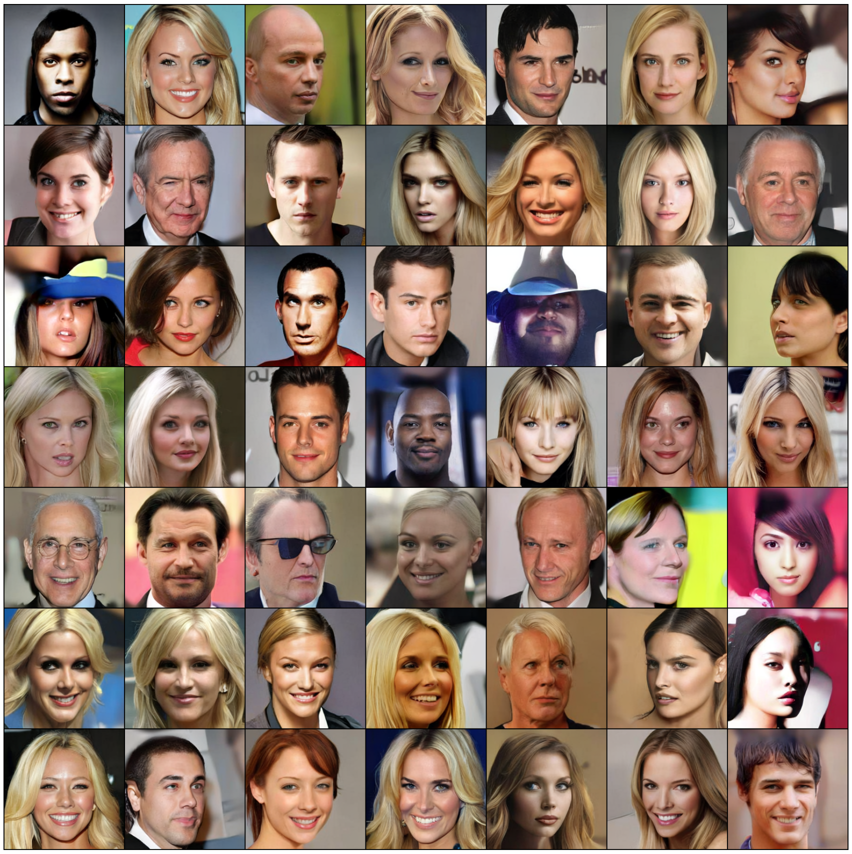

Figure 8: Samples generated by CDRL model trained on the CelebAHQ (256×256) dataset.

D Model Analysis

In this section, we employ several experiments to analyze the CDRL model.

D.1 Ablation Study

In this section, we conduct an ablation study to analyze the effectiveness of each component of our CDRL model. We have previously described three main techniques in our main paper that contribute significantly to our CDRL model: (1) the new noise schedule design, (2) the cooperative training algorithm, and (3) noise variance reduction. We demonstrate the impact of each of these techniques by comparing our CDRL model with the following models:

1. The original diffusion recovery likelihood (DRL) model (Gao et al., 2021) as a baseline.
2. A model trained without using the cooperative training. This corresponds to the DRL but using the same noise schedule and conditioning input as CDRL.
3. CDRL without using noise reduction.
4. Similar to Xiao et al. (2022), we use the initializer to predict the clean image $\hat{\mathbf{x}}_0$ and then transform it to $\hat{\mathbf{y}}_t$. Note that our CDRL uses the initializer to directly predict $\hat{\mathbf{y}}_t$.
5. Similar to Ho et al. (2020), we use initializer to directly output the prediction of total added noise $\hat{\epsilon}$ and then transform it to $\hat{\mathbf{y}}_t$.
6. Compared with the noise schedule used in the original DRL(Gao et al., 2021) paper, the proposed one used in our CDRL places more emphasis on the high-noise area where $\bar{\alpha}$ is close to 0. We train a CDRL model with the original DRL noise schedule but with 2 additional noise levels in the high-noise region for comparison.

7. As depicted in Equation 8 in the main paper, our cooperative training algorithm involves the initializer learning from the revised sample $\tilde{\mathbf{y}}_t$ at each step. A natural question arises: should we instead regress it directly on the data $\mathbf{y}_t$? To answer this, we train a model, in which the initializer directly learns from $\mathbf{y}_t$ at each step.

We ensure that all models share the same network structure and training settings on the CIFAR-10 dataset and differ only in the aforementioned ways. As shown in Table 9, our full model performs the best among these settings, which justifies our design choices.

Table 9: Ablation study on the CIFAR-10 dataset.

Models	**FID** $\downarrow$
DRL (Gao et al., 2021)	9.58
CDRL without cooperative training	6.47
CDRL without noise reduction	5.51
CDRL with an initializer that predicts $\hat{\mathbf{x}}_0$	5.17
CDRL with an initializer that predicts $\hat{\epsilon}$	4.95
CDRL using a noise schedule in DRL-T8	4.94
CDRL with an initializer that learns from $\mathbf{y}_t$	5.95
CDRL (full)	4.31

D.2 Effects of Number of Noise Levels and Number of Langevin Steps

We test whether the noise level can be further reduced. The results in Table 10a show that further reducing noise level to 4 can make model more unstable, even if we increase the number of the Langevin sample steps K. On the other hand, reducing T to 5 yields reasonable but slightly worse results. In Table 10b, we show the effect of changing the number of Langevin steps K. The results show that, on one hand, decreasing K to 10 yields comparable but slightly worse results. On the other hand, increasing K to 30 doesn't lead to better results. This observation aligns wit the finding from Gao et al. (2021). The observation of changing K implies that simply increasing the number of Langevin steps doesn't significantly enhance sample quality, thereby verifying the effectiveness of the initializer in our model.

Table 10: Comparison of CDRL models with varying numbers of noise levels T and varying numbers of Langevin steps K. FIDs are reported on the Cifar-10 dataset.

(a) Results of CDRL models with varying T

Model	FID $\downarrow$
$T = 4$ ($K = 15, 20, 30$)	not converge
$T = 5$ ($K = 15$)	5.08
$T = 6$ ($K = 15$)	4.31

(b) Results of CDRL models with varying K

Model	FID $\downarrow$
$T = 6$ ($K = 10$)	4.50
$T = 6$ ($K = 15$)	4.31
$T = 6$ ($K = 30$)	5.08

D.3 Sampling Time

In this section, we measure the sampling time of CDRL and compare it with the following models: (1) CoopFlow (Xie et al., 2022b), which combines an EBM with a Normalizing Flow model; (2) VAEBM (Xiao et al., 2021), which combines a VAE with an EBM and achieves strong generation performance; (3) DRL (Gao et al., 2021) model with a 30-step MCMC sampling at each noise level. We conduct the sampling process of each model individually on a single A6000 GPU to generate a batch of 100 samples on the Cifar10 dataset. Our CDRL model produces samples with better quality with a relatively shorter time frame. Additionally, with the sampling adjustment techniques, the sampling time can be further reduced without significantly compromising sampling quality.

Table 11: Comparison of different EBMs in terms of sampling time and number of MCMC steps. The sampling time are measured in seconds.

Method	Number of MCMC steps	Sampling Time	FID ↓
CoopFlow (Xie et al., 2022b)	30	2.5	15.80
VAEBM (Xiao et al., 2021)	16	21.3	12.16
DRL (Gao et al., 2021)	6 × 30 = 180	23.9	9.58
CDRL	6 × 15 = 90	12.2	4.31
CDRL (8 steps)	6 × 8 = 48	6.5	4.58
CDRL (5 steps)	6 × 5 = 30	4.2	5.37
CDRL (3 steps)	6 × 3 = 18	2.6	9.67

D.4 Analyzing the Effects of the Initializer and the EBM

To gain deeper insights into the roles of the initializer and the EBM in the CDRL in image generation, we conduct two additional experiments using a pretrained CDRL model on the ImageNet Dataset (32×32). We evaluate two generation options: (a) images generated using only the initializer's proposal, without the EBM's Langevin Dynamics at each noise level, and (b) images generated with the full CDRL model, which includes the initializer's proposal and 15-step Langevin updates at each noise level. As shown in Figure 9a and 9b, the initializer captures the rough outline of the object, while the Langevin updates by the EBM improve the details of the object. Furthermore, in Figure 9c, we display samples generated by fixing the initial noise image and sample noise of each initializer proposal step. The outcomes demonstrate that images generated with the same initialization noises share basic elements but differ in details, highlighting the impact of both the initializer and the Langevin sampling. The initializer provides a starting point, while the Langevin sampling process enriches details.

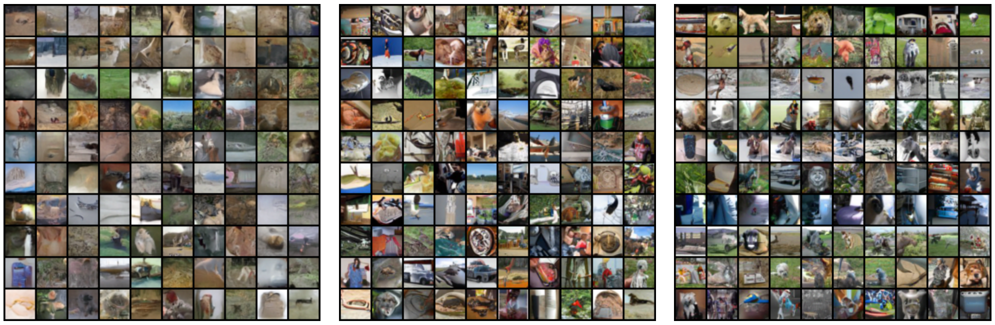

(a) Initializer only (b) Full CDRL model (c) Fixing the initialization noise

Figure 9: Illustration of the effects of the initializer and the EBM on the image generation process using a CDRL model pretrained on the ImageNet Dataset (32×32). (a) Samples generated using only the proposal of the initializer; (b) Samples generated by the full CDRL model; (c) Samples generated by fixing the initial noise image and the sample noise of each initialization proposal step. Each row of images shared the same initial noise image and the sample noise of each initialization proposal step, but differed in the noises of Langevin sampling process at each noise level.

D.5 Analyzing Learning Behavior

We dive into a deeper understanding of the learning behavior of the cooperative learning algorithm. We follow the analysis framework of Xie et al. (2020; 2022a). Let $K_\theta(\mathbf{y}_t|\mathbf{y}_t{}', \mathbf{x}_{t+1})$ be the transition kernel of the K-step Langevin sampling that refines the initial output $\mathbf{y}_t{}'$ to the refined output $\mathbf{y}_t$. Let $(K_\theta q_\phi)(\mathbf{y}_t|\mathbf{x}_{t+1}) = \int K_\theta(\mathbf{y}_t|\mathbf{y}'_t, \mathbf{x}_{t+1}) q_\phi(\mathbf{y}'_t|\mathbf{x}_{t+1}) d\mathbf{y}'_t$ be the conditional disribution of $\mathbf{y}_t$, which is obtained by K steps of Langevin sampling starting from the output of the initialier $q_\phi(\mathbf{y}_t|\mathbf{x}_{t+1})$. Let $\pi(\mathbf{y}_t|\mathbf{x}_{t+1})$ be the true conditional distribution for denoising $\mathbf{x}_{t+1}$ to retrieve $\mathbf{y}_t$. The maximum recovery likelihood for the EBM in Equation 4 in the main paper is equivalent to minimizing the

Kullback-Leibler divergence (KL) divergence $\mathrm{KL}(\pi(\mathbf{x}_t|\mathbf{y}_{t+1})||p_\theta(\mathbf{x}_t|\mathbf{y}_{t+1}))$. Using j to index the learning iteration for model parameters, given the current initializer model $q_\phi(\mathbf{y}_t|\mathbf{x}_{t+1})$, the EBM updates its parameters θ by minimizing

$$\theta_{j+1} = \arg\min_\theta \mathrm{KL}(\pi(\mathbf{y}_t|\mathbf{x}_{t+1})||p_\theta(\mathbf{y}_t|\mathbf{x}_{t+1})) - \mathrm{KL}((K_{\theta_j}q_\phi)(\mathbf{y}_t|\mathbf{x}_{t+1})||p_\theta(\mathbf{y}_t|\mathbf{x}_{t+1})) \tag{21}$$

which is a modified contrastive divergence. It is worth noting that, in the original contrastive divergence, the above $(K_{\theta_j}q_\phi)(\mathbf{y}_t|\mathbf{x}_{t+1})$ is replaced by $(K_{\theta_j}\pi)(\mathbf{y}_t|\mathbf{x}_{t+1})$. That is, the MCMC chains are initialized by the true data. The learning shifts $p_\theta(\mathbf{y}_t|\mathbf{x}_{t+1})$ toward the true distribution $\pi(\mathbf{y}_t|\mathbf{x}_{t+1})$.

On the other hand, given the current EBM, the initializer model learns from the output distribution of the EBM's MCMC. That is, we train the initializer with $\tilde{\mathbf{y}}$ in equation 8 of the main paper. The update of the parameters of the initializer at learning iteration $j+1$ approximately follows the gradient of

$$\phi_{j+1} = \arg\min_\phi \mathrm{KL}(K_\theta q_{\phi_j}(\mathbf{y}_t|\mathbf{x}_{t+1})||q_\phi(\mathbf{y}_t|\mathbf{x}_{t+1})) \tag{22}$$

The initializer $q_\phi(\mathbf{y}_t|\mathbf{x}_{t+1})$, which is a conditional top-down generator, learns to be the stationary distribution of the MCMC transition $K_\theta(\mathbf{x}_t|\mathbf{y}_{t+1})$ by adjusting its mapping towards the low-energy regions of $p_\theta(\mathbf{x}_t|\mathbf{y}_{t+1})$. In a limit, the initializer $q_\phi(\mathbf{y}_t|\mathbf{x}_{t+1})$ minimizes $\mathrm{KL}(K_\theta q_{\phi_j}(\mathbf{y}_t|\mathbf{x}_{t+1})||q_\phi(\mathbf{y}_t|\mathbf{x}_{t+1}))$ and approach the conditional EBM $p_\theta(\mathbf{x}_t|\mathbf{y}_{t+1})$. The entire learning algorithm can be viewed as a chasing game, where the initialzier model $q_\phi(\mathbf{y}_t|\mathbf{x}_{t+1})$ chases the EBM $p_\theta(\mathbf{y}_t|\mathbf{x}_{t+1})$ in pursuit of the true conditional distribution $\pi(\mathbf{y}_t|\mathbf{x}_{t+1})$.

According to the above learning behavior, we can now discuss the benefits of the cooperative learning compared to directly training the initializer with observed $\mathbf{y}$.

Firstly. as presented in Equation 22, the MCMC process of the EBM drives the evolution of the initializer, which seeks to amortize the MCMC. At each learning iteration, in order to provide good initial examples for the current EBM's MCMC, the initialzer needs to be sufficiently close to the EBM. Therefore, training the initialzer with the MCMC outputs $\tilde{\mathbf{y}}$ is a beneficial strategy to maintain a appropriate distance between EBM and initialzer model. Conversely, if the initializer directly learns from the true distribution, even though it may move toward the true distribution quickly, it might not provide a good starting point for the MCMC. A competent initializer should assist in identifying the modes of the EBM. Consider a scenario in which the initizlier model initially shifts toward the true distribution by learning directly from $\mathbf{y}$, but the EBM remains distant. Due to a large divergence between the EBM and the initialzier, the latter may not effectively assist the EBM in generating fair samples, especially with finite-step Lanegevin dynamics. A distant initializer could lead to unstable training of the EBM.

Secondly, let us consider a more general senario where our initializer is modeled using a non-Gaussian generator $\mathbf{y}_t = g_\phi(\mathbf{x}_{t+1}, \mathbf{z}, t)$, where $\mathbf{z} \sim \mathcal{N}(0, \boldsymbol{I})$ introduces randomness through the latent vector $\mathbf{z}$. In this case $q_\phi(\mathbf{y}_t|\mathbf{x}_{t+1}) = \int p(\mathbf{y}_t|\mathbf{x}_{t+1}, \mathbf{z})p(\mathbf{z})d\mathbf{z}$ is analytically intractable. Learning $q_\phi(\mathbf{y}_t|\mathbf{x}_{t+1})$ directly from $\mathbf{y}$ independently requires MCMC inference for the posterior distribution $q_\phi(\mathbf{z}|\mathbf{x}_{t+1}, \mathbf{y}_t)$. However, cooperative learning circumvents the challenge of inferring the latent variables $\mathbf{z}$. That is, at each learning iteration, we generate examples $\hat{\mathbf{y}}$ from $q_\phi(\mathbf{y}_t|\mathbf{x}_{t+1})$ by first sampling $\hat{\mathbf{z}} \sim p(\mathbf{z})$ and then mapping it to $\hat{\mathbf{y}}_t = g_\phi(\mathbf{x}_{t+1}, \hat{\mathbf{z}}, t)$. The $\hat{\mathbf{y}}$ is used to initialze the EBM's MCMC that produces $\tilde{\mathbf{y}}$. The learning equation of ϕ is $\frac{1}{n}\sum_{i=1}^n -\frac{1}{2\tilde{\sigma_t}^2}||\tilde{\mathbf{y}}_{t,i} - g_\phi(\mathbf{x}_{t+1,i}, \hat{\mathbf{z}}, t)||^2$, where the latent variables $\hat{\mathbf{z}}$ is used. That is, we shift the mapping from $\hat{\mathbf{z}} \to \hat{\mathbf{y}}$ to $\hat{\mathbf{z}} \to \tilde{\mathbf{y}}$ for accumulating the MCMC transition. Although our paper currently employs a Gaussian initializer, if we adopt a more expressive non-Gaussian initializer in the future, the current cooperative learning strategy (i.e., training q_ϕ with $\tilde{\mathbf{y}}$) can be much more beneficial and feasible.

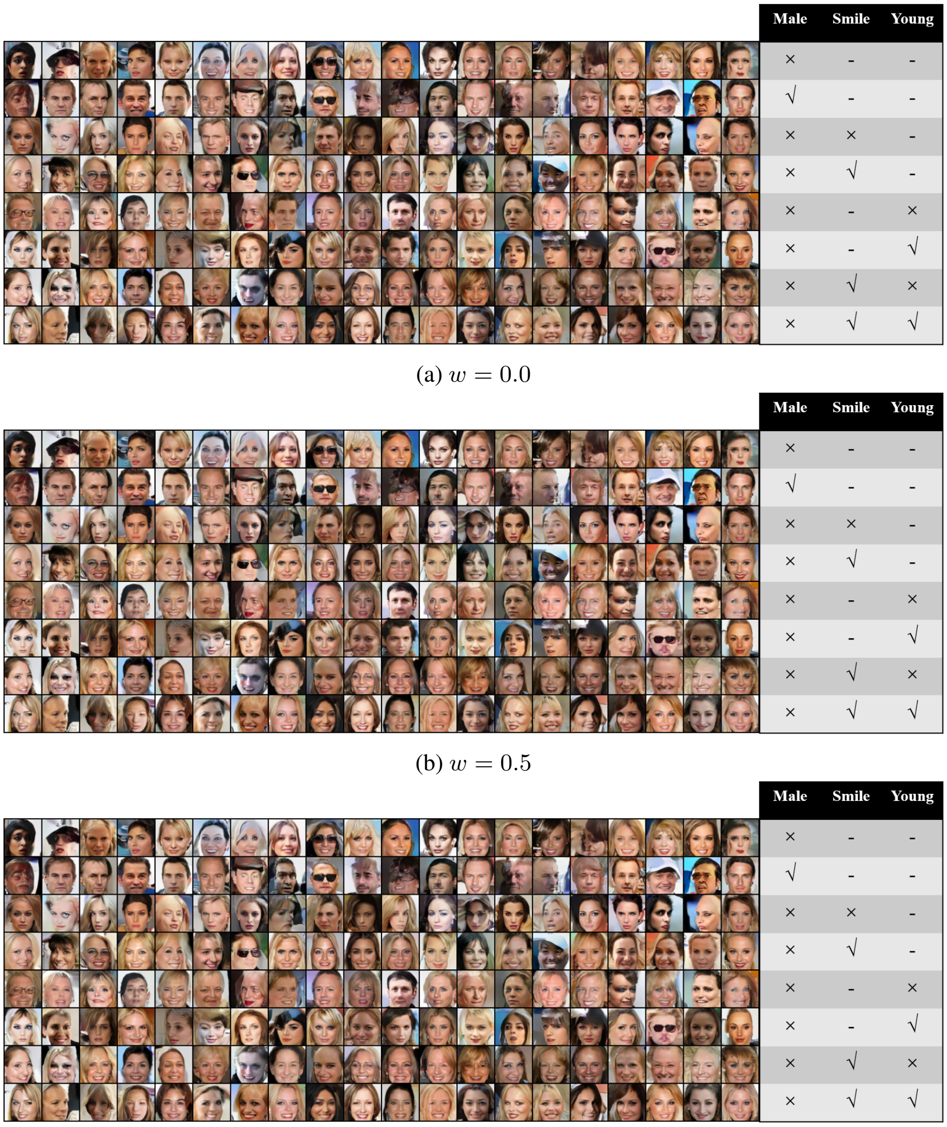

(a) $w = 0.0$

(b) $w = 0.5$

(c) $w = 1.0$

Figure 10: Attribute compositional samples generated by CDRL models trained on the CelebA (64×64) dataset. We utilize guided weights $w = 0.0, 0.5, 1.0$. Images at different guidance share the same random noise. Results can also be compared with those in Figure 4, which use $w = 3.0$.

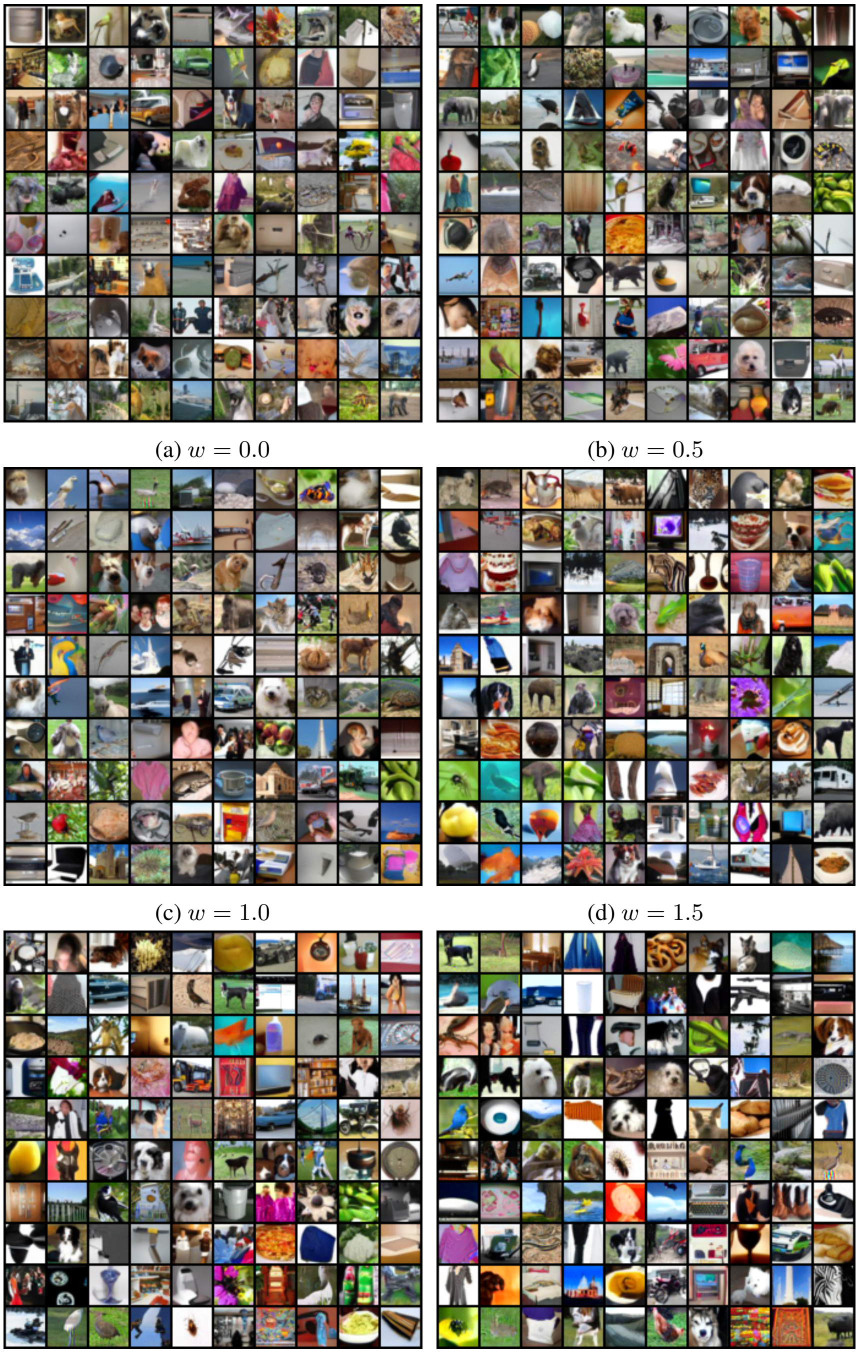

(a) $w = 0.0$

(b) $w = 0.5$

(c) $w = 1.0$

(d) $w = 1.5$

(e) $w = 2.0$

(f) $w = 3.0$

Figure 11: Conditional generated examples with various classifier-free guidance weights on the ImageNet32 (32 × 32) dataset. Samples are generated using randomly selected class labels.

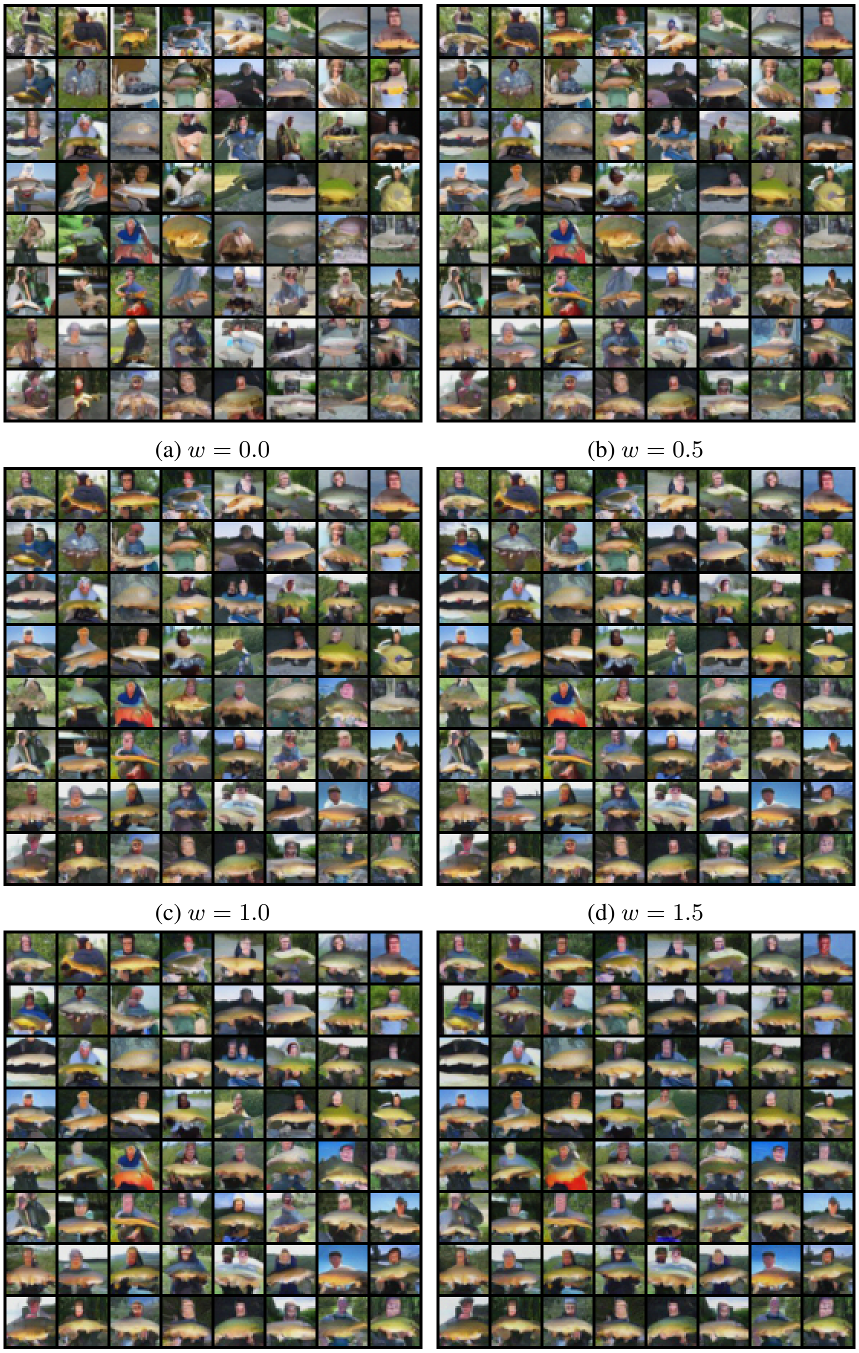

(a) $w = 0.0$

(b) $w = 0.5$

(c) $w = 1.0$

(d) $w = 1.5$

(e) $w = 2.0$

(f) $w = 3.0$

Figure 12: Conditional generated examples with different classifier-free guidance weights on the ImageNet32 (32 × 32) dataset, using the class label "Tench".

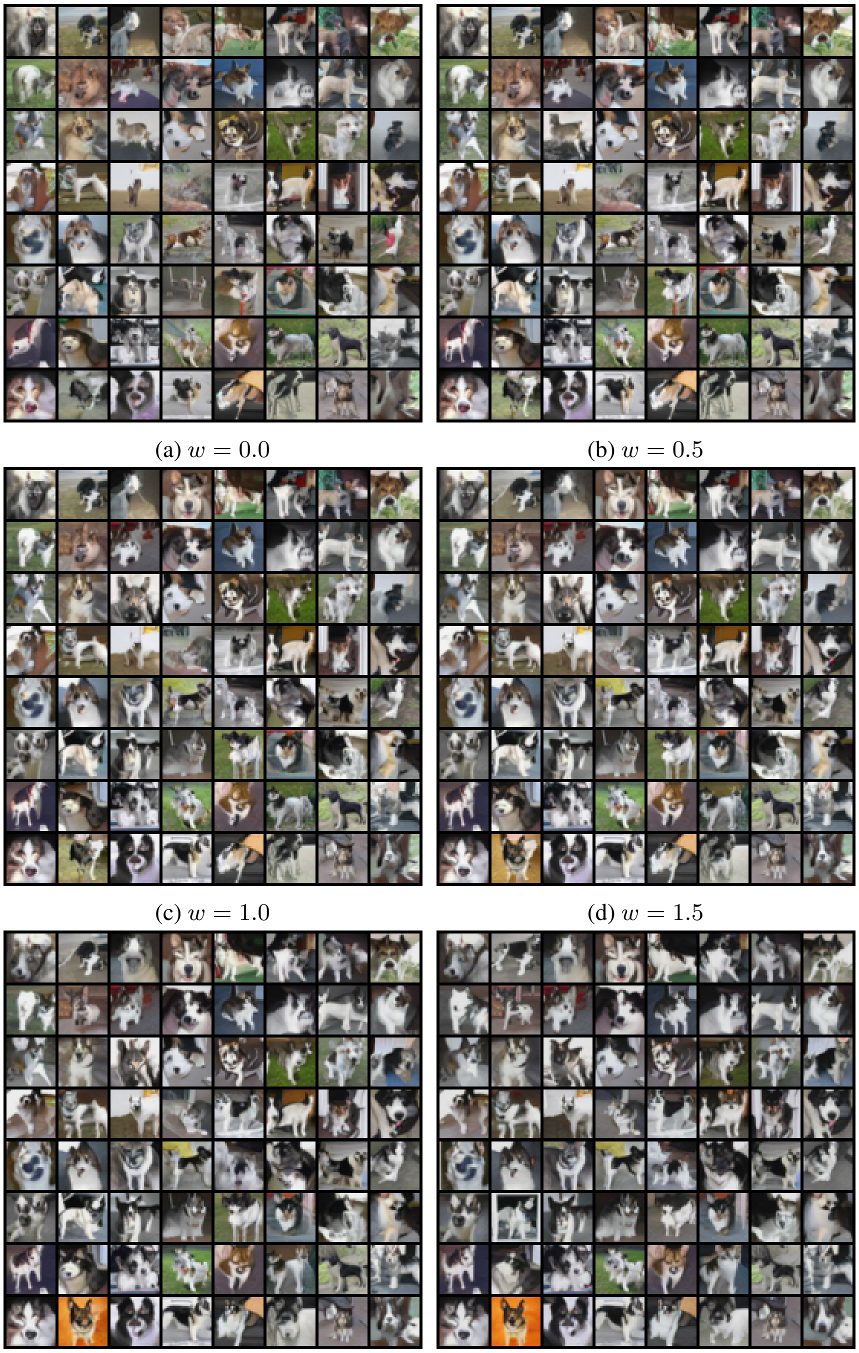

(a) $w = 0.0$

(b) $w = 0.5$

(c) $w = 1.0$

(d) $w = 1.5$

(e) $w = 2.0$

(f) $w = 3.0$

Figure 13: Conditional generated examples with different classifier-free guidance weights on the ImageNet32 (32 × 32) dataset, using the class label "Siberian Husky".

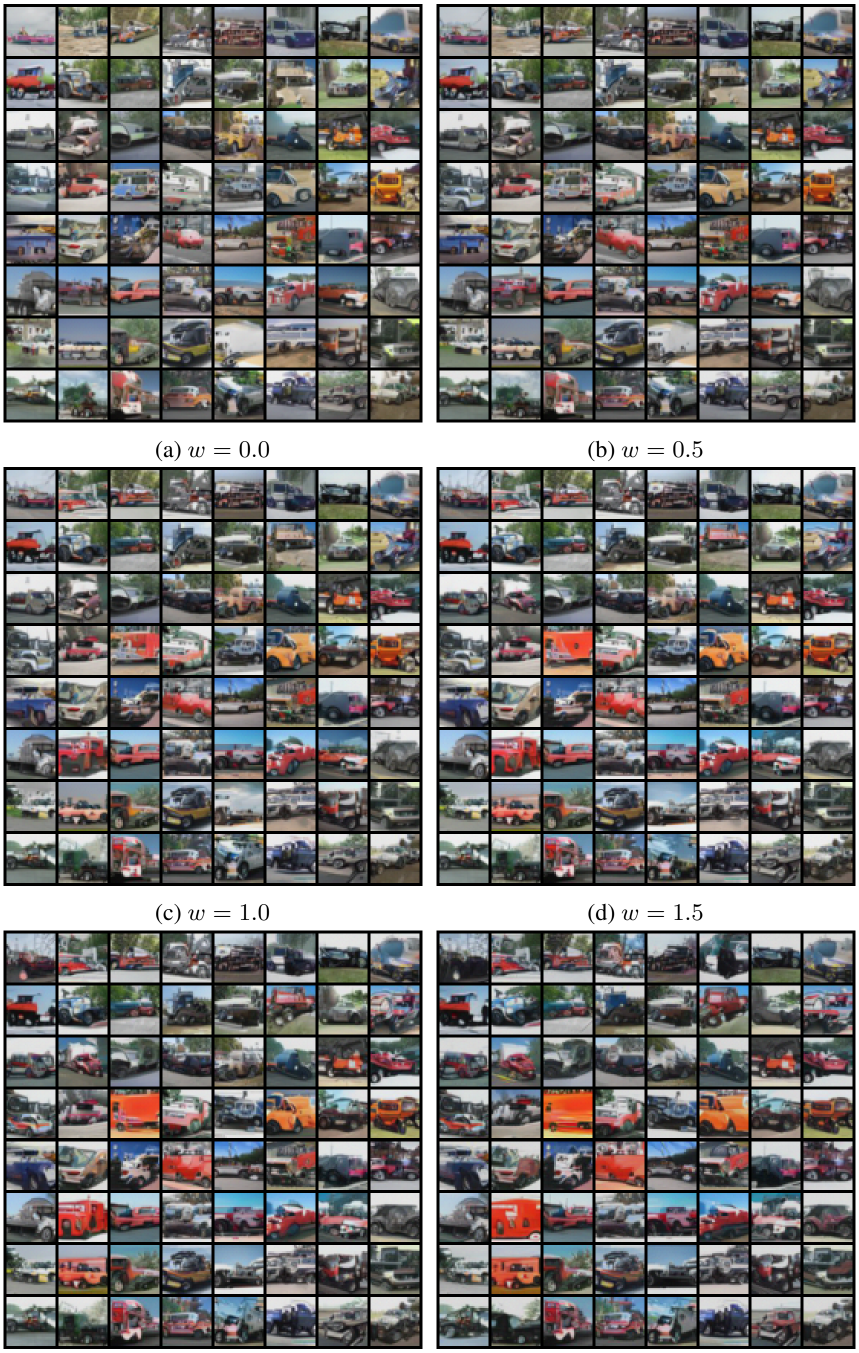

(a) $w = 0.0$

(b) $w = 0.5$

(c) $w = 1.0$

(d) $w = 1.5$

(e) $w = 2.0$

(f) $w = 3.0$

Figure 14: Conditional generated examples with different classifier-free guidance weights on the ImageNet32 (32 × 32) dataset, using the class label "Tow Truck".

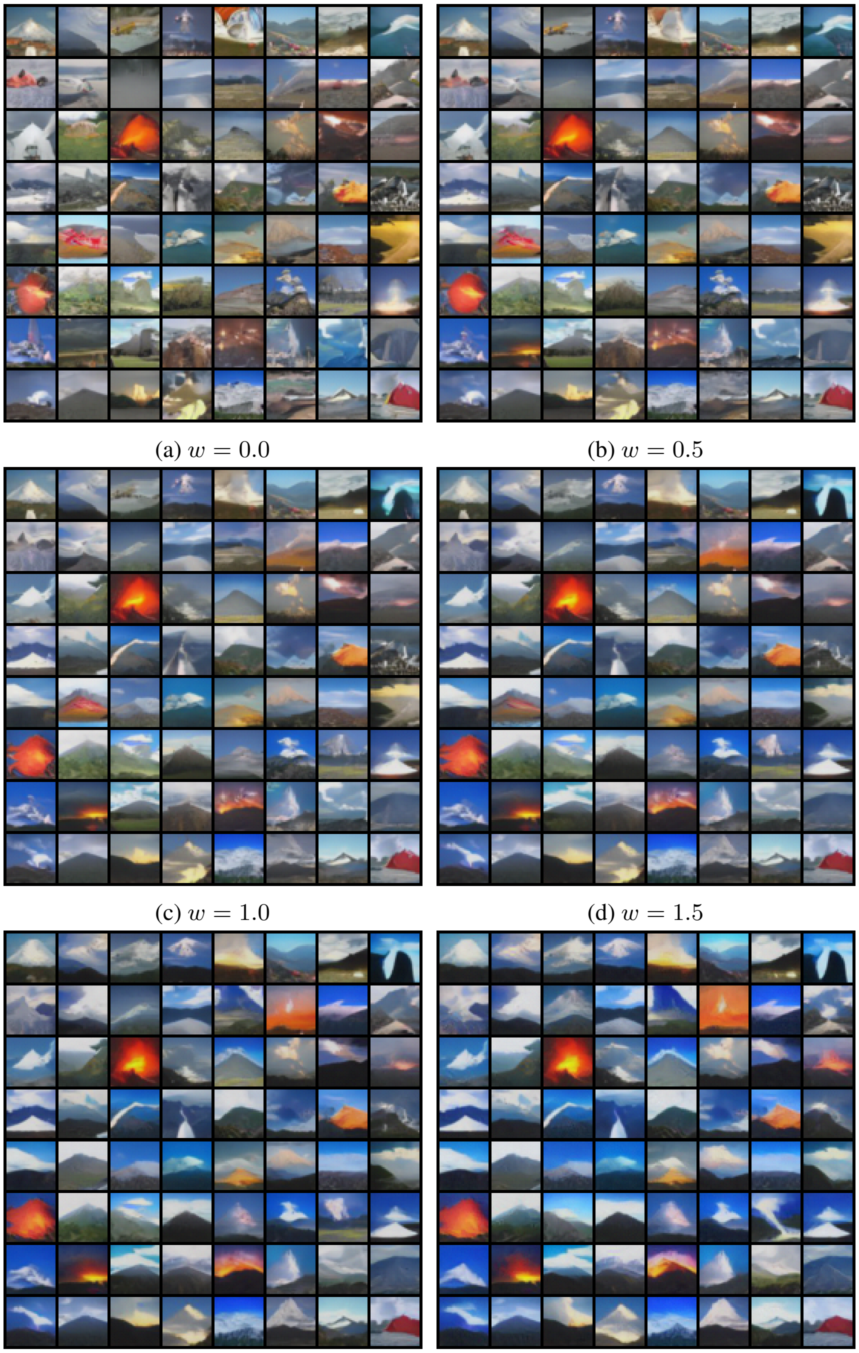

(a) $w = 0.0$

(b) $w = 0.5$

(c) $w = 1.0$

(d) $w = 1.5$

(e) $w = 2.0$

(f) $w = 3.0$

Figure 15: Conditional generated examples with different classifier-free guidance weights on the ImageNet32 (32 × 32) dataset, using the class label “Volcano”.